Biol Cybern (2009) 101:147–167
DOI 10.1007/s00422-009-0326-5

ORIGINAL PAPER

Biological Cybernetics

Stability switches, oscillatory multistability, and spatio-temporal patterns of nonlinear oscillations in recurrently delay coupled neural networks

Yongli Song · Valeri A. Makarov · Manuel G. Velarde

Received: 21 January 2009 / Accepted: 2 July 2009 / Published online: 21 July 2009

Abstract A model of time-delay recurrently coupled spatially segregated neural assemblies is here proposed. We show that it operates like some of the hierarchical architectures of the brain. Each assembly is a neural network with no delay in the local couplings between the units. The delay appears in the long range feedforward and feedback inter-assemblies communications. Bifurcation analysis of a simple four-units system in the autonomous case shows the richness of the dynamical behaviors in a biophysically plausible parameter region. We find oscillatory multistability, hysteresis, and stability switches of the rest state provoked by the time delay. Then we investigate the spatio-temporal patterns of bifurcating periodic solutions by using the symmetric local Hopf bifurcation theory of delay differential equations and derive the equation describing the flow on the center manifold that enables us determining the direction of Hopf bifurcations and stability of the bifurcating periodic orbits. We also discuss computational properties of the system due to the delay when an external drive of the network mimicks external sensory input.

Keywords Neural network · Delay · Hopf bifurcation · Stability · Spatio-temporal pattern

Y. Song · V. A. Makarov · M. G. Velarde
Instituto Pluridisciplinar, Universidad Complutense,
Paseo Juan XXIII, 1, 28040 Madrid, Spain

Y. Song
Department of Mathematics, Tongji University,
200092 Shanghai, China

V. A. Makarov (✉)
Depto. de Matemática Aplicada, Facultad de Matemáticas,
Universidad Complutense, Avda. Complutense s/n,
28040 Madrid, Spain
e-mail: vmakarov@mat.ucm.es

1 Introduction

Transmission delay seems to play a significant role in integration of information arriving to a single neuron in different spatial and temporal windows and also at the network level in interneuron communication. The delay can cancel or amplify multiple spikes thus leading to the neural information being selectively processed. The theoretical study of the dynamics of simple units organized into networks with delayed couplings revealed a rich variety of possible scenarios of transition to a global oscillatory behavior induced by the delay (see, e.g., Bungay and Campbell 2007; Campbell et al. 2005; Guo 2005; Guo and Huang 2003; Guo 2007; Huang and Wu 2003; Song et al. 2005; Wu et al. 1999; Wu 1998; Yuan and Campbell 2004; Yuan 2007; Wei et al. 2002; Wei and Velarde 2004 and references therein). The emerging oscillations can exhibit different spatio-temporal patterns sensitive to the delay. It has been shown that even small, comparing to the oscillation period, delays may have a large impact on the dynamics of pulse-coupled integrate and fire oscillators (Ernst et al. 1995; Gerstner 1996; Timme et al. 2002a,b) and lead, e.g., to the coexistence of regular and irregular dynamics (Timme et al. 2002b).

Research on Hopfield-type neural networks with delays, first introduced by Marcus and Westervelt (1989), has also shown that delay can drastically modify the global dynamics of the system. Since then delays have been inserted into various simple neural networks. Among the most widely studied phenomena is synchronization, where individual units oscillate at common frequency and phase when coupled. In Ikeda and Matsumoto (1987), Schuster and Wagner (1989), Niebur et al. (1991), Ramana Reddy et al. (1998), Ramana Reddy et al. (1999), Seunghwan et al. (1997), and Song et al. (2007), the authors studied the time evolution of coupled limit cycle oscillators with time delay. The vast majority of these works

is devoted to investigation of neural-like networks possessing linear or circular overall symmetry (units coupled in a one-dimensional (1D) lattice or in a ring). However, the neural networks found in the brain are far from being symmetric. As a matter of fact, the brain organization can be viewed in gross sense as a number of local subnetworks (gray matter) coupled by long distance connections (white matter) (Braitenberg and Schuz 1998; Kandel et al. 2000). Another important observation is that neural networks in the brain rarely can be considered autonomous, but instead subjected to external input or drive. Recently, Campbell et al. (2004) investigated the stability and bifurcations in the delayed neural network of two coupled three-neuron subnetworks.

The block-like brain structures can be identified in different sensory pathways. For instance, in the somatosensory system dorsal column nuclei (DCN) neurons form a complex compact oscillatory network receiving sensory inputs. Only part of the neurons in DCN project to the thalamus and subsequently the sensory information (SI) goes to the cortex. In turn DCN receive corticofugal fibers through the pyramidal tract (see, e.g., Jabbur and Towe 1961; Valverde 1966) thus closing the loop. The cortical feedback locally is mediated through excitatory synapses, while its effective global action is inhibitory. This may happen due to corticofugal primary excitation of inhibitory interneurons. Recent experimental findings (Castellanos et al. 2007; Malmierca et al. 2009) indicate that a descending feedback significantly alters (modulates) the oscillatory and information processing properties of DCN. The functional coupling between the sensory stimulus and the neural response in DCN exhibits infra-slow oscillation (about 0.07 Hz). During this oscillation the stimulus coherence can temporarily fall below the statistically significant level, i.e., the functional stimulus-response coupling may be temporarily lost for a single neuron. Activation of the corticofugal feedback rescues the functional coupling of DCN projecting neurons to the stimulus. This suggests that the processing of the sensory input occurs at the network level, while firing of individual neurons may be unreliable.

Although evolution might maximize brain functionality by shortening conduction delays (see discussion in Wen and Chklovskii 2005 and references therein), for modeling purpose we can assume that the transmission delay occurring in the long scale (inter-block) communications is significantly longer than the local delays occurring among the interneurons belonging to the same subnetwork (block). Besides, one can argue that the presence of short intra-block delays may be "absorbed" by the longer inter-block delays, such that the global circuit dynamics of a Hopfield-like neural circuit will depend on the global composite delay (see, e.g., Wei et al. 2002; Wei and Velarde 2004 and references therein). Then the dynamics of the complete network is expected to be robust against introducing small but non-zero intra-block delays. Thus the interneuron short-distance delays can be neglected in a first approximation. Figure 1a illustrates a rather general architecture with two local subnetworks A and B recurrently coupled with delays. We assume that the neurons inside each block (subnetwork) communicate with no delay. Each of such structures can be considered as a generator of local field potential (LFP), while the long distance coupling provides a means for driving, synchronization and/or modulation of the oscillatory pattern by the other neural assembly. The bottom neuron assembly A also receives an external input that conveys SI. We shall refer to such a system as a recurrently delayed coupled neural network (RDCNN).

Recent experimental results show the feasibility of simultaneous multi-site recordings and posterior deconvolution of the oscillatory activity of different local neural assemblies in the rat hippocampus (Makarov et al. 2009), known to be responsible for spatial information storage (Kandel et al. 2000). It was found that under different experimental conditions LFP generators (subnetworks) may show in-phase or delayed activity, which suggests the presence of a coupling and also points to a possible nontrivial role of the delay. Thus the study of RDCNNs may also shed light into the memory functioning.

The paper is organized as follows. In Sect. 2, we introduce a minimal model capturing the main architectural properties of a sensory pathway with mixed (delayed and instantaneous) interactions. Then in Sects. 3 and 4 we provide its bifurcation analysis and discuss the computational properties of the system by studying the response of the network to external stimuli. Finally Sect. 5 summarizes our results.

2 A minimal model of RDCNN

As a first approximation to the general problem of delayed interaction of spatially separated neural assembles (Fig. 1a) here we consider two delayed coupled subnetworks, each consisting of two neurons recurrently coupled with no delay (Fig. 1b). The first subnetwork A receives an external input $s(t)$, processes it and sends further to the subnetwork B, which in turn modulates the dynamics of the subnetwork A through the feedback. Such simplified scheme resembles the main architectural properties of the somatosensory pathway. To describe the dynamics of individual neurons and synaptic couplings we adopt here the Hopfield-like neural network paradigm. Accordingly, the governing equations are given by

$$\text{A:}\begin{cases}\dot{x}_1(t) = -x_1(t) + a_{12} f(x_2(t)) + c_b f(y_2(t-\tau_b))\\ \dot{x}_2(t) = -x_2(t) + a_{21} f(x_1(t)) + s(t)\end{cases}$$

$$\text{B:}\begin{cases}\dot{y}_1(t) = -y_1(t) + b_{12} f(y_2(t)) + c_f f(x_2(t-\tau_f))\\ \dot{y}_2(t) = -y_2(t) + b_{21} f(y_1(t))\end{cases} \tag{1}$$

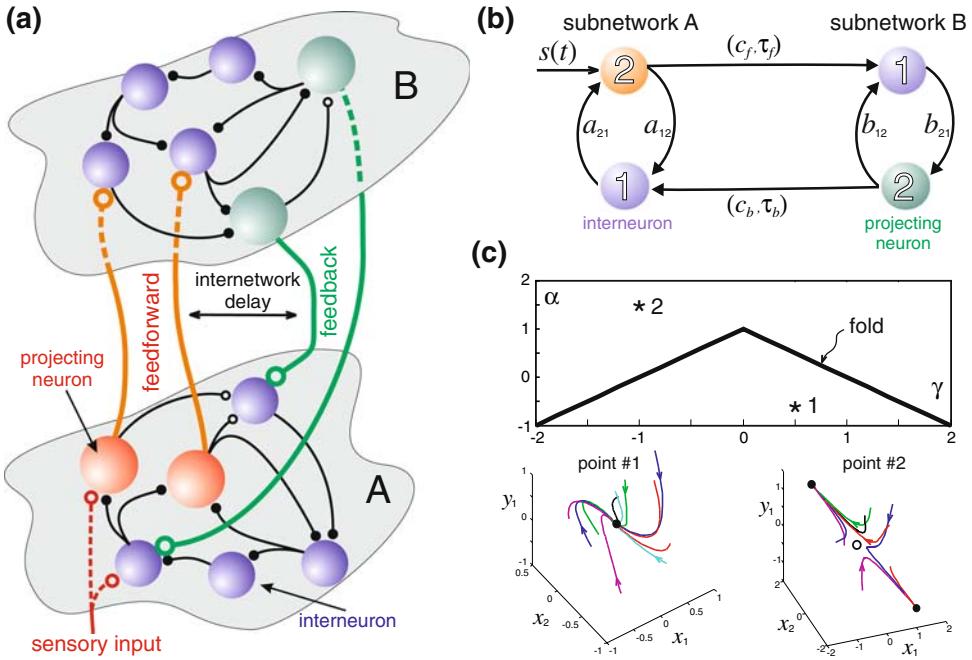

Fig. 1 **a** Architecture of recurrently delayed coupled neural networks (RDCNN) resembling the structural organization of a sensory pathway. The system consists of two subnetworks A and B coupled through feedforward and feedback links. Neurons inside each local subnetwork interact with no delay, while the long range couplings produce a delay in signal propagation between subnetworks. To model sensory input, the "low level" network A also may receive an external sensory input. *Open* and *filled* terminals correspond to excitatory and inhibitory synapses. **b** Minimal model of RDCNN. Two subnetworks consisting of two Hopfield-like neurons are recurrently coupled with delays $\tau_{f,b}$. $s(t)$ is an external drive. **c** Partitioning of the parameter space into domains with qualitatively different behaviors in the zero delay limit and symmetric case $\beta = \alpha$ (*top*). The parameter space is divided by a fold bifurcation into two domains with monostable and bistable behaviors of the network. The bottom diagrams show two examples of the 3D phase space projections. Stable steady states are marked by *filled circles*, whereas the *open circle* corresponds to an unstable (saddle) steady state

where x and y account for the neuron trans-membrane voltages in the subnetworks A and B, respectively; a_{ij} and b_{ij} denote the coupling strengths within the local networks; and $c_{f,b}$ are the *feedforward* and *feedback* long range coupling weights. For a positive coupling $a_{ij} > 0$, the jth neuron is called excitatory and inhibitory otherwise ($a_{ij} < 0$). In (1) the delays $\tau_{f,b}$ occur in the internetwork couplings only. The external input to the network A is given by the time dependent function $s(t)$. Further to describe the phase space of (1) we shall also use vector representation:

$$u = (x_1, x_2, y_1, y_2)^{\mathrm{T}} \tag{2}$$

The synaptic (transfer) function $f : \mathbb{R} \to \mathbb{R}$ is assumed to be sufficiently smooth and sigmoidal (e.g., $f(x) = \tanh(x)$ is used for computer simulations). For the stability analysis we shall only require

$$f \in C^1(\mathbb{R}), \quad f(0) = 0, \quad f'(0) = 1 \tag{3}$$

whereas, for the bifurcation analysis we additionally assume

$$f \in C^3(\mathbb{R}), \quad f''(0) = 0, \quad f'''(0) \neq 0 \tag{4}$$

The particular function $f(x) = \tanh(x)$ satisfies both conditions with $f'''(0) = -2$.

In the uncoupled case, i.e., when the two subnetworks do not communicate with each other, $c_{f,b} = 0$, the individual dynamics of the independent subnetworks is determined by the *local composite gains*

$$\alpha = a_{12}a_{21}, \quad \beta = b_{12}b_{21} \tag{5}$$

Without external input, for

$$\alpha < 1 \text{ (or } \beta < 1 \text{ for B)}$$

the zero solution $x_1 = x_2 = 0$ (or $y_1 = y_2 = 0$ for B) or rest state is asymptotically stable and unstable otherwise. One can show that in the latter case the subnetwork is bistable. Besides the unstable (saddle) steady state in the origin, the system has two symmetric stable steady states $(\bar{x}_1, \bar{x}_2)$ and $(-\bar{x}_1, -\bar{x}_2)$. Depending on the initial conditions trajectories in the phase space tend to one or the other state. Thus recurrently inhibitory (both $a_{12,21} < 0$) or excitatory ($a_{12,21} > 0$) subnetworks with strong enough synapses ($\alpha > 1$) are switchable, i.e., applying an appropriate stimulus one can switch the network from one state to the other.

In the coupled case ($c_f \neq 0$, $c_b \neq 0$), similarly to (5) it is useful to define the *global composite gains*

$$\gamma_b = a_{21}c_b, \quad \gamma_f = b_{21}c_f \tag{6}$$

As we shall discuss later on, a RDCNN without delay ($\tau_{f,b} \to 0$) in the symmetric case ($\beta = \alpha, \gamma_b = \gamma_f = \gamma$, and $s(t) = 0$) has asymptotically stable zero solution $u = 0$ if

$$\alpha < 1 - |\gamma|$$

otherwise the system shows multistability. Thus connecting two subnetworks decreases the region of global stability of the rest state $u = 0$. Figure 1c illustrates two sections of the parameter space and shows examples of typical trajectories for the two qualitatively different behaviors.

For the sake of simplicity we shall restrict the study of the network (1) to the symmetric case, i.e., we assume:

$$a_{12} = b_{12}, \quad a_{21} = b_{21}, \quad c_f = c_b = c, \quad \tau_f = \tau_b = \tau \tag{7}$$

Then the local and global composite gains are pairwise equal, i.e., $\beta = \alpha$ and $\gamma_b = \gamma_f = \gamma$. In the reminder of the paper we shall focus on the effect of the time delay τ on the dynamics of the system (1). Generally speaking, long enough time delay may cause nonlinear oscillations in the network. Most of these oscillations appear in the form of periodic solutions with certain spatio-temporal structure and, if stable under small perturbations, offer a kind of associative memory of the network (Fuchs and Haken 1988) such that information can be stored and later retrieved. We first explicitly obtain the conditions guaranteeing stability of the rest state ($u = 0$) and then investigate Hopf bifurcations and the spatio-temporal patterns of the bifurcating periodic solutions. We also provide numerical bifurcation analysis using DDE-BIFTOOL v. 2.03 (Engelborghs et al. 2001) and custom software written in Matlab. Finally, computational network properties (response to external input) are discussed.

3 Bifurcations of the rest state

3.1 Steady states

In the case of a constant external drive $s(t) = s_0$ the steady states of (1) are given by

$$\begin{aligned} u_1^* &= a_{12} f(u_2^*) + c f(u_4^*) \\ u_2^* &= a_{21} f(u_1^*) + s_0 \\ u_3^* &= a_{12} f(u_4^*) + c f(u_2^*) \\ u_4^* &= a_{21} f(u_3^*) \end{aligned} \tag{8}$$

Depending on the parameter values, (8) can have from one to nine solutions. If $s_0 = 0$ then (8) always has the zero solution $u^* = 0$ or the rest state.

3.2 Global stability

By constructing a Lyapunov functional we obtain the following theorem on the global stability of the rest state $u^* = 0$ of the system (1).

Theorem 1 *The zero solution of the system (1) with $s(t) = 0$ is globally asymptotically stable if the transfer function fulfills (3), $f \in C^2(\mathbb{R})$, and $f''(x)x < 0$ for all $x \neq 0$ and $|a_{12}| + |a_{21}| + |c| < 2$.*

The proof of Theorem 1 is given in Appendix A.

Remark 1 If the external input to the network is nonzero though a constant, i.e., $s_0 \neq 0$, and $u^*(s_0)$ is a steady state of (1) given by (8), then by changing variables, $\hat{u} = u - u^*(s_0)$ we translate the system (1) into new coordinates with the steady state $\hat{u}^* = 0$. Then the stability of the steady state u^* of the system (1) is equivalent to the stability of the zero solution of the translated system. The arguments very similar to given in the proof of Theorem 1 yield that if the transfer function fulfills $f'(u_j^*) = 0$ and $f''(u_j^* + \epsilon)\epsilon < 0$ for any $\epsilon \neq 0$ ($j = 1, 2, 3, 4$) then the steady state u^* of the system (1) is globally asymptotically stable for any constant input s_0.

3.3 Stability of zero solution and Hopf bifurcations induced by delay

We assume no external input, i.e., $s(t) = 0$. Then linearization of the autonomous system (1) around the zero solution $u^* = 0$ yields

$$\dot{u}(t) = M_1 u(t) + M_2 u(t - \tau) \tag{9}$$

where

$$M_1 = \begin{pmatrix} -1 & a_{12} & 0 & 0 \\ a_{21} & -1 & 0 & 0 \\ 0 & 0 & -1 & a_{12} \\ 0 & 0 & a_{21} & -1 \end{pmatrix}, \quad M_2 = \begin{pmatrix} 0 & 0 & 0 & c \\ 0 & 0 & 0 & 0 \\ 0 & c & 0 & 0 \\ 0 & 0 & 0 & 0 \end{pmatrix} \tag{10}$$

The *characteristic matrix* of the linear system (9) is given by

$$\Delta(\tau, \lambda) = \lambda I - M_1 - e^{-\lambda\tau} M_2$$

Then the characteristic equation determining the local stability of the zero solution can be written as

$$\det \Delta(\tau, \lambda) = \Delta_+ \cdot \Delta_- = 0 \tag{11}$$

where

$$\Delta_\pm = \lambda^2 + 2\lambda + 1 - \alpha \pm \gamma e^{-\lambda\tau} \tag{12}$$

Clearly, λ is a root of (11) if and only if either of the equations $\Delta_+ = 0$ and $\Delta_- = 0$ is fulfilled. These equations

belong to the class of the transcendental polynomial equation

$$\lambda^2 + p\lambda + r + qe^{-\lambda\tau} = 0 \quad (q \neq 0) \tag{13}$$

which has been extensively studied (see, e.g., Ruan 2001; Song et al. 2004). In Appendix B, we recall the main results on (13) related to our analysis. Comparing (12) and (13), one gets

$$p = 2, \quad r = 1 - \alpha, \quad q = \begin{cases} \gamma & \text{for } \Delta_+ \\ -\gamma & \text{for } \Delta_- \end{cases} \tag{14}$$

For $\tau = 0$, i.e., with no delay in the feedforward and feedback loops (Fig. 1), the four roots of (11) are:

$$\lambda_{1,2,3,4} = -1 \pm \sqrt{\alpha \pm |\gamma|}$$

These roots have negative real parts if the following inequality holds

$$\alpha < 1 - |\gamma| \tag{15}$$

In other words, the trivial solution of the coupled system (1) is asymptotically stable if and only if the condition (15) is satisfied. Thus increasing the strength (modulus) of the internetwork coupling c we can always make the rest state unstable through a fold bifurcation. Figure 1c shows the parameter space and examples of typical trajectories for the non-delayed case.

For nonzero time delay ($\tau > 0$) we introduce:

$$\tau_0^{\pm} = \frac{1}{\omega_\pm} \arccos\left(\frac{\omega_\pm^2 + \alpha - 1}{|\gamma|}\right) \tag{16}$$

where

$$\omega_\pm = \sqrt{-1 - \alpha \pm \sqrt{\gamma^2 + 4\alpha}} \tag{17}$$

Note that $\omega_\pm$ and $\tau_0^{\pm}$ make sense only when real, i.e., in a limited parameter domain. Then the characteristic equation (11) is fulfilled for (see Appendix B):

$$\tau_j^{\pm} = \tau_0^{\pm} + \frac{j\pi}{\omega_\pm}, \quad j = 0, 1, 2, \ldots \tag{18}$$

As we shall discuss further below, it is convenient to sort the values $\tau_j^{\pm}$ in the ascending order. Using the fact that $\omega_+ > \omega_-$ we get

$$\tau_0^+ < \tau_0^- \tag{19}$$

The sequence of τ for $j = 1, 2, \ldots$ depends on the parameter values, e.g., for $\alpha = -4$, $\gamma = 4.2$

$$\tau^+ \approx 0.84, 2.36, 3.88, \ldots; \quad \tau^- \approx 1.88, 4.28, 6.67, \ldots \tag{20}$$

hence, $\tau_0^+ < \tau_0^- < \tau_1^+ < \tau_2^+ < \tau_1^- < \cdots$.

Let us now introduce on the (α, γ)-plane, four domains counterparts of the domains A1-A3 introduced in Appendix B (Fig. 2a):

$$D_1 = \left\{(\alpha, \gamma) \,\middle|\, \alpha < -1,\ 2\sqrt{|\alpha|} < \gamma < 1 - \alpha\right\}$$

$$D_2 = \left\{(\alpha, \gamma) \,\middle|\, \alpha < -1,\ \alpha - 1 < \gamma < -2\sqrt{|\alpha|}\right\}$$

$$D_3 = \left\{(\alpha, \gamma) \,\middle|\, \left(\alpha \leq -1,\ |\gamma| < 2\sqrt{|\alpha|}\right) \cup \left(|\alpha| < 1,\ |\gamma| < 1 - \alpha\right)\right\}$$

$$D_4 = \mathbb{R}^2 - \overline{D_1 \cup D_2 \cup D_3}$$

where $\overline{D}$ denotes the closure of the domain D. Using Lemma 6 from Appendix B and (18) we obtain the following result on the distribution of roots of the characteristic equation (11).

Lemma 1 (i) *If $(\alpha, \gamma) \in D_4$, then the characteristic equation (11) has at least one pair of roots with positive real parts*

(ii) *If $(\alpha, \gamma) \in D_3$, then all roots of (11) have negative real parts for $\tau \geq 0$*

(iii) *If either $\alpha < -1$ and $\gamma = \pm 2\sqrt{|\alpha|}$ or $|\gamma| > |1 - \alpha|$, then (11) has a pair of simple purely imaginary roots $\lambda = \pm i\omega_+$ at $\tau = \tau_j^+$*

(iv) *If $(\alpha, \gamma) \in D_1 \cup D_2$ and $\tau_0^- > \tau_1^+$, then all roots of (11) have negative real parts for $\tau \in [0, \tau_0^+)$ and at least a pair of roots with positive real parts for $\tau > \tau_0^+$.*

(v) *If $(\alpha, \gamma) \in D_1 \cup D_2$ and $\tau_0^- < \tau_1^+$, then there is a positive integer k such that all roots of (11) have negative real parts for*

$$\tau \in [0, \tau_0^+) \cup (\tau_0^-, \tau_1^+) \cup \cdots \cup (\tau_{k-1}^-, \tau_k^+)$$

but for

$$\tau \in (\tau_0^+, \tau_0^-) \cup (\tau_1^+, \tau_1^-) \cup \cdots \cup (\tau_{k-1}^+, \tau_{k-1}^-)$$

there is a pair of roots with positive real parts, and at least a pair of roots with positive real parts for $\tau > \tau_k^+$. Moreover, for $\tau = \tau_j^+$ (respectively $\tau = \tau_j^-$), $j = 0, 1, 2, \ldots, k$ all roots of (11) have negative real parts, except for a pair of simple purely imaginary roots $\lambda = \pm i\omega_+$ (respectively $\lambda = \pm i\omega_-$).

(vi) *If $\alpha < -1$ and $|\gamma| = |1 - \alpha|$, then the characteristic equation (11) has at least one root $\lambda = 0$ and a pair of simple roots $\lambda = \pm i\sqrt{-2(1 + \alpha)}$ at $\tau = \tau_j^+$. Moreover: if $\alpha \geq -1$ and $\alpha \neq 1$, $\tau \neq \frac{2}{|\gamma|}$, then $\lambda = 0$ is a single root; if $(\alpha, \gamma) = (1, 0)$ or $\alpha > 1$, $|\gamma| = \alpha - 1$ and $\tau = \frac{2}{|\gamma|}$, then $\lambda = 0$ is a double root.*

Using Lemma 1, the transversality condition (37) and the Hopf bifurcation theorem for functional differential equa-

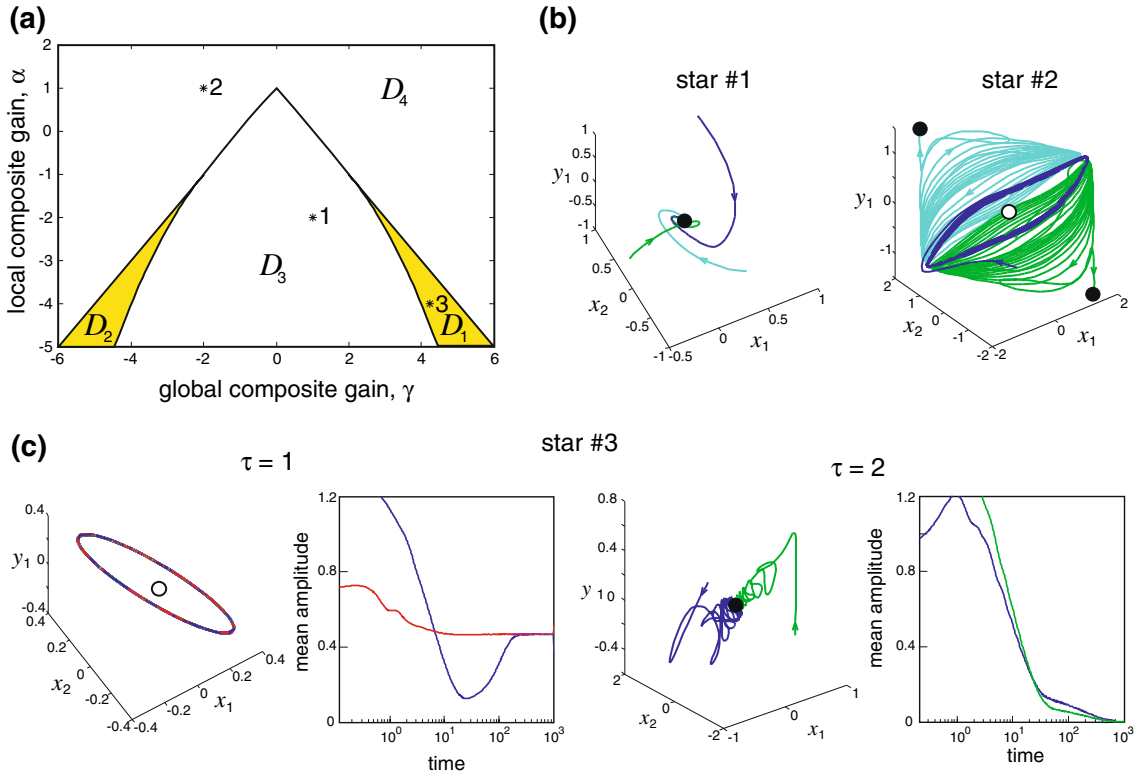

Fig. 2 **a** Parameter plane of the RDCNN (1) with symmetric architecture. In the region D_3, the rest state $u^* = 0$ is asymptotically stable for all $\tau \geq 0$. It is unstable in D_4 for any τ. If $(\alpha, \gamma) \in D_1 \cup D_2$, then the stability depends on the delay. There are windows for the delay τ where the trivial solution is either stable or unstable. **b** Examples of two phase space projections for parameters from D_3 (star #1 in **a**: $\alpha = -2$, $\gamma = 1$, $\tau = 1$) and from D_4 (star #2 in **a**: $\alpha = 1$, $\gamma = -2$, $\tau = 4$). The asymptotic behavior is similar to the network without delay (Fig. 1c). However, the transient behavior differs, e.g., in D_4 a long decaying oscillation is observed. The decay can last hundreds of oscillation periods. **c** Examples of phase space projections (only final parts of trajectories are shown) and time evolution of the oscillation amplitude for the parameters from D_2 (star #3 in **a**: $\alpha = -4$, $\gamma = 4.2$). The *left inset* corresponds to the value of τ inside an unstable window, whereas the right one is for $\tau = 2$ which belongs to a stable window

tions (Hale et al. 1993), we obtain the following result on the stability and bifurcations of the rest state in the system (1).

Theorem 2 *Assume that* α, γ, $\omega_\pm$ *and* $\tau_j^\pm$ *are defined by (5), (6), (17), and (18), respectively. Then for any time delay* $\tau \geq 0$ *the rest state* $u^* = 0$ *of the RDCNN (1) is unstable for* $(\alpha, \gamma) \in D_4$, *and it is asymptotically stable for* $(\alpha, \gamma) \in D_3$.

For $(\alpha, \gamma) \in D_1 \cup D_2$*:*

(i) *If* $\tau_0^- > \tau_1^+$, *the rest state is asymptotically stable for* $\tau \in [0, \tau_0^+)$ *and unstable for* $\tau > \tau_0^+$.

(ii) *If* $\tau_0^- < \tau_1^+$, *then there is a positive integer* k *such that the rest state is asymptotically stable for*

$$\tau \in [0, \tau_0^+) \cup (\tau_0^-, \tau_1^+) \cup \cdots \cup (\tau_{k-1}^-, \tau_k^+)$$

and unstable for

$$\tau \in (\tau_0^+, \tau_0^-) \cup (\tau_1^+, \tau_1^-) \cup \cdots \cup (\tau_{k-1}^+, \tau_{k-1}^-) \cup \tau > \tau_k$$

The RDCNN (1) undergoes a Hopf bifurcation at: i) $\tau = \tau_j^\pm$ *if* $(\alpha, \gamma) \in D_1 \cup D_2$*; and ii)* $\tau = \tau_j^+$ *if* $|\gamma| > |1 - \alpha|$.

Figure 2a shows the splitting of the (γ, α) parameter plane into regions with qualitatively different behaviors of the RDCNN. In regions D_3 and D_4 the asymptotic behaviors are qualitatively similar to the corresponding behaviors shown in Fig. 1c for the network without delay. In D_3 the perturbations decay to $u^* = 0$ (Fig. 2b, left inset), whereas in D_4 we have bistability (Fig. 2b, right inset). The difference with the non-delayed case appears in the transient dynamics. Particularly, in D_4 for sufficiently long delay the trajectories can oscillate for a long time around the unstable trivial solution $u^* = 0$ before approaching one of the stable steady states.

Relative to the non-delayed case (Fig. 1c) two new regions D_1 and D_2 appear in the parameter plane (Fig. 2a). The network dynamics in these regions significantly depends on the actual delay value. One of the conclusions of Theorem 2 is that for appropriate parameter values along the delay axis τ there exist k switches from stability to instability and back

to stability. This means that the rest state of the RDCNN can be switched from stable to unstable and back to stable and so on just by progressive increase of the delay in the feedforward and feedback couplings. Such changes may occur in the somatosensory pathway, e.g., during development. Figure 2c shows two examples with opposite behaviors obtained for the same parameter values of the local and global composite couplings but for different delays. Noteworthy is that the oscillatory behavior can be observed for a lower delay ($\tau = 1$ in Fig. 2c) than the delay values ($\tau = 2$ in Fig. 2c) at which the trivial solution $u^* = 0$ is globally asymptotically stable. Such surprising behavior will be further analyzed in Sect. 4.

When the parameters α and γ fulfill one of the conditions of Lemma 1 (item *vi*) the qualitative behavior of solutions of (1) in the neighborhood of the origin is quite complex, leading to a Bogdanov–Takens bifurcation and steady-state/Hopf collision.

3.4 Direction and stability of Hopf bifurcations

Theorem 2 provides conditions on the parameter values (including delay) at which the trivial solution $u^* = 0$ of the system (1) undergoes Hopf bifurcations. Besides, it also states that there is no Hopf bifurcation in the domain D_3 (Fig. 2a). For $(\alpha, \gamma) \in D_4$, Lemma 1 ensures that the characteristic equation (11) has at least one pair of roots with positive real parts. Thus for $|\gamma| > |1 - \alpha|$ (region D_4) the limit cycles emanating from Hopf bifurcations are unstable in the whole phase space (although they may be stable on a central manifold). Figure 2b (right inset) also indirectly confirms this. Indeed, rotating trajectories suggest that there is a saddle type limit cycle surrounding the origin. Trajectories stay for a long time nearby the limit cycle but finally leave the region towards one of the two stable steady states. Thus similarly to the non-delayed case (Fig. 1c) the RDCNN can show bistability in this region, but the transient behavior can be oscillatory. However, as we shall show in Sect. 4 the evolution of the RDCNN could be more complex than its non-delayed counterpart, as expected.

In the remainder of this section we shall consider Hopf bifurcations of the steady state $u^* = 0$ occurring in the region $D_1 \cup D_2$.

We denote the critical value of the time delay at Hopf bifurcation by τ_*, and define a new bifurcation parameter

$$\mu = \tau - \tau_* \tag{21}$$

According to Theorem 2, for $\mu = 0$ the characteristic equation (11) has a pair of purely imaginary roots $\lambda = \pm i\omega_0$ with ω_0 given by (17): ω_+ for τ_j^+ and ω_- for τ_j^-. Without loss of generality, in this section we assume that the transfer function satisfies both inequalities (3) and (4). Then, following the procedure based on the center manifold theorem and normal form reduction described by Faria and Magalhães (1995a,b) we determine the direction and stability of Hopf bifurcations by deriving explicitly the normal form of the system (1) on the associated 2D center manifold at $\mu = 0$ (Appendix C):

$$\begin{aligned} \dot{\varrho} &= K_1\mu\rho + K_2\rho^3 + \mathcal{O}\left(\mu^2\rho + |(\rho,\mu)|^4\right) \\ \dot{\xi} &= -\Omega + \mathcal{O}(|(\rho,\mu)|) \end{aligned} \tag{22}$$

where (ϱ, ξ) are the polar coordinates in the 2D manifold, $\Omega = \omega_0\tau_*$ is the oscillation frequency, and $K_{1,2}$ are constants defined by (59) and (60), respectively:

$$\begin{aligned} K_1 &= \Re(A_1) = -4\omega_0\Im(\hat{u}) \\ K_2 &= \Re(A_2) = \frac{1}{2}f'''(0)\tau_*\|v\|^2\left(\Re(\hat{u}) - \omega_0\Im(\hat{u})\right) \end{aligned} \tag{23}$$

where $\hat{u}$ is given by (53). Denoting

$$\Pi = f'''(0)\left(\Re(\hat{u}) - \omega_0\Im(\hat{u})\right) \tag{24}$$

we also have $K_2 = \tau_*\|v\|^2\Pi/2$.

The sign of the product K_1K_2 determines the direction of the Hopf bifurcation (Chow and Hale 1982). The bifurcation is supercritical for $K_1K_2 < 0$ and subcritical if $K_1K_2 > 0$. The sign of K_2 determines stability of the emanating periodic orbit. The orbit is stable for $K_2 < 0$, and unstable for $K_2 > 0$.

To determine the signs of $K_{1,2}$ we use (53) and (17). The latter equation can also be written as $\omega_0^2 + 1 = -\alpha \pm 2\sqrt{\gamma^2 + 4\alpha}$. For $\alpha < 0$ (required for the existence of the domains D_1 and D_2, Fig. 2a) we obtain

$$\Re(\hat{u}) = 2|\hat{u}|^2\left(2 + \tau_* - \frac{\tau_*\alpha}{\omega_0^2 + 1}\right) > 0$$

$$-\omega_0\Im(\hat{u}) = \frac{2\tau_*\omega_0^2|\hat{u}|^2\left(\pm 2\sqrt{\gamma^2 + 4\alpha}\right)}{\omega_0^2 + 1} \begin{cases} > 0, & \text{for } \tau_* = \tau_j^+ \\ < 0, & \text{for } \tau_* = \tau_j^- \end{cases}$$

which together with (23) yield

$$K_1 > 0, \quad \text{for } \tau_* = \tau_j^+, \quad \text{and} \quad K_1 < 0, \quad \text{for } \tau_* = \tau_j^- \tag{25}$$

and

$$\operatorname{sgn}(K_2) = \begin{cases} \operatorname{sgn}(f'''(0)), & \text{for } \tau_* = \tau_j^+ \\ \operatorname{sgn}(\Pi), & \text{for } \tau_* = \tau_j^- \end{cases} \tag{26}$$

Equations (25) and (26) directly lead to the following theorem.

Theorem 3 *If the transfer function $f(\cdot)$ satisfies (3) and (4), and the composite couplings $(\alpha, \gamma) \in D_1 \cup D_2$, then the direction of the Hopf bifurcations of $u^* = 0$ and stability of the bifurcating periodic solutions are determined by:*

(i) *the sign of $f'''(0)$ at $\tau = \tau_j^+$. If $f'''(0) < 0$ (> 0, respectively), then the Hopf bifurcations occurring on*

the center manifold of (1) are supercritical (subcritical, respectively), with non-trivial periodic orbits stable (unstable, respectively) on the center manifold.

(ii) *by the sign of Π at $\tau = \tau_j^-$. If $\Pi < 0$ (> 0, respectively), then the Hopf bifurcations occurring on the center manifold of (1) are subcritical (supercritical, respectively), with non-trivial periodic orbits stable (unstable, respectively) on the center manifold.*

The condition (ii) of Theorem 3 can be simplified. Indeed, for $\tau = \tau_j^-$ we can estimate the second term of Π:

$$\begin{aligned}\Re(\hat{u})-\Im(\hat{u})\omega_- &= 2|\hat{u}|^2\left(2+\tau_j^-+\tau_j^-\omega_-^2+\tau_j^-\alpha\frac{\omega_-^2-1}{\omega_-^2+1}\right)\\ &> 2|\hat{u}|^2\left(2+\tau_j^-+\tau_j^-\omega_-^2+\tau_j^-\alpha\right)\\ &= 4|\hat{u}|^2\left(1-\tau_j^-\sqrt{\gamma^2+4\alpha}\right)\end{aligned}$$

Thus, assuming that $\tau_j^- < 1/\sqrt{\gamma^2+4\alpha}$ and $f'''(0) < 0$ (respectively, >0), the Hopf bifurcations for $u^* = 0$ occurring on the center manifold of (1) at $\tau = \tau_j^-$ are subcritical (respectively, supercritical), with non-trivial periodic orbits stable (respectively, unstable) on the center manifold.

The stability and direction of Hopf bifurcations can be determined for almost all critical values τ_j^- when (α, γ) is on or sufficiently close to the curve $\alpha = -\gamma^2/4$.

Remark 2 Lemma 1 ensures that the characteristic equation (11) has at least one root with positive real part for $(\alpha, \gamma) \in D_1 \cup D_2$ and $\tau > \tau_k$. Thus, in this case the bifurcating periodic orbits are always unstable even though they may be stable on the center manifold.

Remark 3 The stability of the bifurcating periodic solutions on the center manifold coincides with that in the whole phase space only for $(\alpha, \gamma) \in D_1 \cup D_2$ with the critical values $\tau_j^\pm$ if $j \le k$.

Remark 4 From (37), (39), item (iii) of Lemma 1, the normal form (22) with (25) and (26), we also obtain that for $-\infty < \alpha < -1$ and $\gamma = \pm\sqrt{-4\alpha}$ the zero solution of the system (1) is stable for $\tau \ge 0$.

The particular function $f(x) = \tanh(x)$ has negative third derivative ($f'''(0) = -2$). Thus using Theorem 3 we obtain that the Hopf bifurcations occur at the right neighborhood of τ_j^+, and the bifurcating periodic solutions are stable on the center manifold.

3.5 Spatio-temporal patterns of bifurcating periodic solutions

Let us now investigate the spatio-temporal patterns of bifurcating periodic solutions emanating from Hopf bifurcations discussed above. Through this section we shall use the notation introduced in Wu (1998).

Let $G : C \to \mathbb{R}^n$ and Γ be a compact group. Then the dynamical system

$$\dot{u}(t) = G(u_t)$$

is Γ-equivariant if $G(\rho(u_t)) = \rho G(u_t)$ for all $\gamma \in \Gamma$ (Wu 1998; Golubitsky et al. 2003). Let $\Gamma = Z_2$ be a cyclic group of order 2. Denoting the generator of this group by γ, its action on $\mathbb{R}^4$ is given by

$$\rho(u_i) = u_{i+2}, \quad \text{for all } i \ (\text{mod}4) \quad \text{and} \quad u \in \mathbb{R}^4 \tag{27}$$

Lemma 2 *The RDCNN (1) in the symmetric case (7) is Z_2 equivariant.*

Proof Let $G(u_t) = L_\tau(u_t) + F(u_t, \tau)$ as defined in (42). Then, for the generator ρ of Z_2, by (27) it is straightforward to verify that $G(\rho(u_t)) = \rho G(u_t)$. This completes the proof.

Linear functional differential equations generate a strongly continuous semigroup of linear operators with infinitesimal generator $A(\tau)$ given by Hale et al. (1993):

$$A(\tau)\varphi = \dot{\varphi}, \quad \varphi \in \text{Dom}(A)$$
$$\text{Dom}(A) = \{\varphi \in C, \ \varphi(0) = L(\tau)\varphi\}$$

with $L(\tau)$ defined in Appendix C:

$$L_\tau = \tau M_1\varphi(0) + \tau M_2\varphi(-1)$$

Moreover, the spectrum $\sigma(A(\tau))$ consists of roots of the characteristic equation (11). Thus using results of Sect. 3.3 (Lemma 1) we obtain:

Lemma 3 *If $(\alpha, \gamma) \in D_1 \cup D_2$ and the characteristic equation (11) has a pair of purely imaginary root $\lambda = \pm i\omega_0$ at $\tau = \tau_*$, where $\tau_* \in \{\tau_j^\pm, \ j = 0, 1, \ldots\}$ and ω_0 is given by ω_+ for τ_j^+ or ω_- for τ_j^-, respectively, then*

(i) *The characteristic matrix $\Delta(\tau, \lambda)$ is continuously differentiable with respect to τ.*

(ii) *The infinitesimal generator $A(\tau)$ of the linear operator $L(\tau)$ has a pair of simple eigenvalues $\lambda = \pm i\omega_0$ at $\tau = \tau_*$. Moreover, the other eigenvalues of $A(\tau_*)$ are not integer multiples of $\pm i\omega_0$.*

(iii) *There exist $\delta_* > 0$ and a smooth curve $\lambda : (\tau_* - \delta_*, \tau_* + \delta_*) \to \mathbb{C}$ such that $\lambda(\tau_*) = i\omega_0$ and $\Delta(\tau, \lambda(\tau)) = 0$ for $\tau \in (\tau_* - \delta_*, \tau_* + \delta_*)$. Moreover, $\frac{d\Re(\lambda)}{d\tau}|_{\tau=\tau_*} \neq 0$ as well as $\dim U_\lambda(A(\tau)) = \dim U_\lambda(A(\tau_*))$ for $\tau \in (\tau_* - \delta_*, \tau_* + \delta_*)$.*

(iv) *The generalized eigenspace $U_{i\omega_0}(A(\tau_*))$, P, of $A(\tau_*)$ for $\pm i\omega_0$ is spanned by the eigenvectors $\Re(e^{i\omega_0\theta}v)$ and $\Im(e^{i\omega_0\theta}v)$, i.e.,*

$$U_{i\omega_0}(A(\tau_*)) = \{x_1\varepsilon_1(\theta) + x_2\varepsilon_2(\theta), \ x_1, x_2 \in \mathbb{R}\}$$

where

$$\varepsilon_1(\theta) = \cos(\omega_0\theta)\Re(v) - \sin(\omega_0\theta)\Im(v)$$
$$\varepsilon_2(\theta) = \sin(\omega_0\theta)\Re(v) + \cos(\omega_0\theta)\Im(v)$$

and v is defined by (51), (52) for j even and odd, respectively.

Let $\omega = \frac{2\pi}{\omega_0}$. We denote by P_ω the Banach space of all continuous ω-periodic mappings of $\mathbb{R}$ into $\mathbb{R}^4$, equipped with the supremum norm. Then, for the circle group S^1, $Z_2 \times S^1$ acts on P_ω by

$$(\rho, e^{i\theta})x(t) = \rho x(t+\theta),\ (\rho, (\theta)) \in Z_2 \times S^1,\ x \in P_\omega$$

Denote by SP_ω the subspace of P_ω consisting of all ω-periodic solutions of (1) at $\tau = \tau_*$. Then

$$SP_\omega = \{x_1\varepsilon_1(t) + x_2\varepsilon_2(t),\ y_1, y_2 \in \mathbb{R}\}$$

For any $\theta \in (0, \omega)$

$$\Sigma^\theta = \left\{\left(\rho, e^{i\frac{2\pi}{\omega}\theta}\right)\right\}$$

is a subgroup of $Z_2 \times S^1$. For Σ^θ, we define the fixed point subspace

$$\mathrm{Fix}(\Sigma^\theta, SP_\omega) = \Big\{x(t) \in SP_\omega;\ (\rho, e^{i\theta})x = x \text{ for all } (\rho, e^{i\theta}) \in \Sigma^\theta\Big\}$$

Lemma 4 *If either $\theta = \left(n + \frac{1}{2}\right)\omega$ for $\Delta_+ = 0$, or $\theta = n\omega$ for $\Delta_- = 0$, where $n \in \mathbb{Z}$, then*

$$\mathrm{Fix}(\Sigma^\theta, SP_\omega) = SP_\omega$$

Otherwise, $\mathrm{Fix}(\Sigma^\theta, SP_\omega) = \{0\}$. *Particularly*

$$\dim \mathrm{Fix}(\Sigma^\theta, SP_\omega) = \begin{cases} 2 & \theta = \left(n + \frac{1}{2}\right)\omega \text{ for } \Delta_+ = 0,\ \text{or } \theta = n\omega \text{ for } \Delta_- = 0 \\ 0 & \text{otherwise} \end{cases}$$

The proof of this lemma is given in Appendix D.

Lemma 5 *Denote the action of $\Gamma = Z_2$ on $\mathbb{R}$ by $\rho(y) = -y$ for $\Delta_+ = 0$, and by $\rho(y) = y$ for $\Delta_- = 0$. Then $\mathbb{R}$ is an absolutely irreducible representation of Γ, and the restricted action of Γ on $\mathrm{Ker}\Delta(\tau_*, i\omega_0)$ is isomorphic to the action of Γ on $\mathbb{R} \oplus \mathbb{R}$.*

The proof of this lemma is given in Appendix 5.

In addition, it follows from (40), (41), and (18) that for a positive global composite coupling $\gamma > 0$ the even and odd subscripts j of $\tau_j^\pm$ are associated with Δ_+ and Δ_-, respectively, but for $\gamma < 0$ they are associated with Δ_- and Δ_+, respectively. This, together with Lemmas 2–5 and the symmetric Hopf bifurcation theorem for DDEs (Wu 1998), immediately lead to the following theorem.

Theorem 4 *Let j be the subscript of $\tau_* = \tau_j^\pm$ defining the bifurcation point, then near τ_* there exists a bifurcation of periodic solutions of the system (1) with the period $P \approx 2\pi/\omega_0$ satisfying:*

(i) *for $(\alpha, \gamma) \in D_1$ or $\gamma > |1 - \alpha|$*

$$u_{i+2}(t) = \begin{cases} u_i\left(t - P/2\right), & \text{if } j \text{ is even} \\ u_i(t), & \text{if } j \text{ is odd} \end{cases} \tag{28}$$

(ii) *for $(\alpha, \gamma) \in D_2$ or $|\gamma| > |1 - \alpha|$ and $\gamma < 0$*

$$u_{i+2}(t) = \begin{cases} u_i\left(t - P/2\right), & \text{if } j \text{ is odd} \\ u_i(t), & \text{if } j \text{ is even} \end{cases} \tag{29}$$

Theorems 3 and 4 ensure that the Hopf bifurcation occurs at the right neighborhood of τ_j^+, and the bifurcating periodic solution is stable on the center manifold. The emanating periodic orbit for j being even is such that the oscillations in the subnetworks A and B are in anti-phase, whereas for j being odd the oscillations are in-phase.

In the case of $\tanh(x)$ using (53) and (23) we obtain that

$$\mathrm{sgn}(K_2) = -\mathrm{sgn}\left(\Re(\hat{u}) - \omega_-\Im(\hat{u})\right) \approx \begin{cases} -\mathrm{sgn}(0.0712) < 0 & \text{for } \tau = \tau_0^- \\ -\mathrm{sgn}(0.0359) < 0 & \text{for } \tau = \tau_1^- \end{cases} \tag{30}$$

Thus at the left neighborhood of τ_0^- the system (1) undergoes a Hopf bifurcation and the bifurcating periodic orbit is stable and corresponds to anti-phase oscillations in the subnetworks A and B. At the left neighborhood of τ_1^- the system (1) also undergoes the Hopf bifurcation and the bifurcating periodic solution is stable but the oscillations are in-phase.

4 Numerical analysis

In this section, we numerically crosscheck and extend the analytical results on the bifurcation analysis of the RDCNN (1) made above. Then we study the network dynamics under a change of parameter values and its response to an external input.

4.1 Bifurcation diagram of the RDCNN

First let us study bifurcations of the steady states and limit cycles. We choose the synaptic strength of the collaterals of the projecting neurons a_{12} (Fig. 1b) as the bifurcation parameter, while the other parameters are fixed: $a_{21} = -2$, i.e., the interneurons are inhibitory in both subnetworks; $c = 2.05$, i.e., projections to the other subnetworks are excitatory; and the internetwork delay is moderate $\tau = 1.5$. Then the global composite coupling is $\gamma = -4.1$, which in turn defines

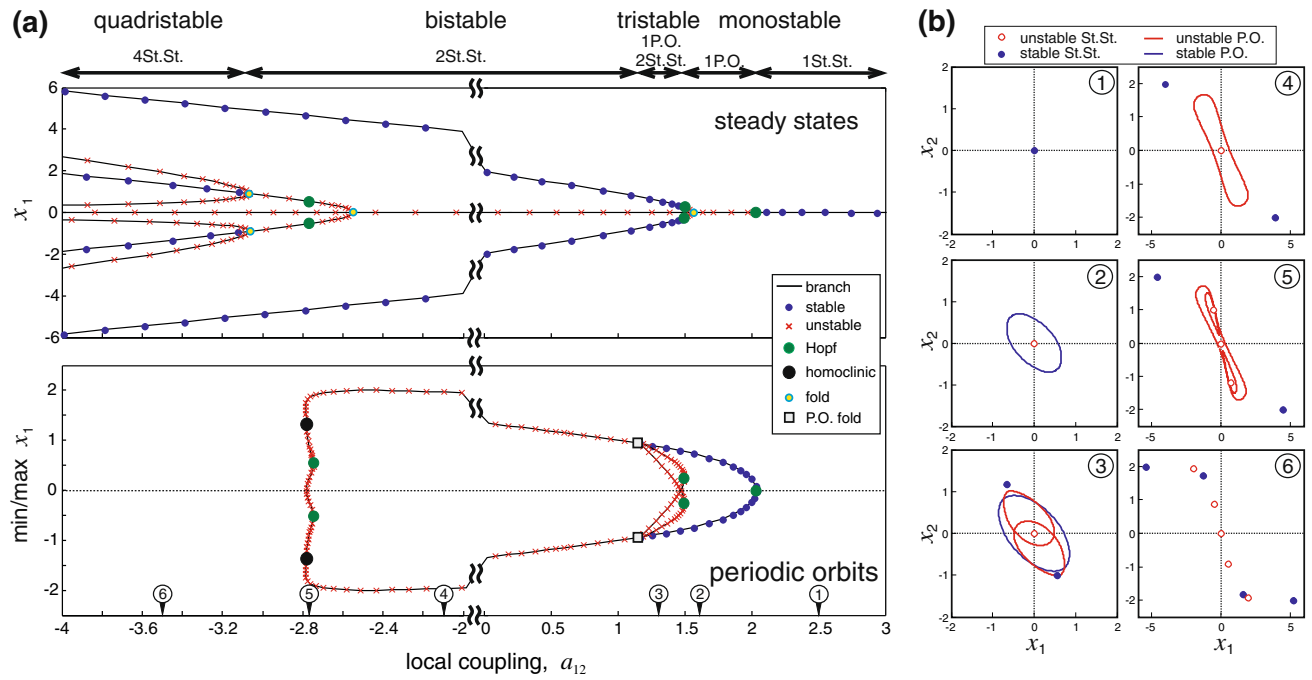

Fig. 3 **a** Bifurcations of steady states (St.St.) (*top*) and periodic orbits (P.O.) (*bottom*) along the parameter a_{12} describing the strength of (local) collateral coupling of the projecting neurons (Fig. 1b) for fixed inter-neuron delay $\tau = 1.5$ ($a_{21} = -2$, $c = 2.05$). The region $-2 < a_{12} < 0$ has no qualitative changes in the behavior of the RDCNN and has been cut out. **b** Projections of steady states and limit cycles in the phase space of (1) into (x_1, x_2)-plane for six representative values of a_{12} marked by cycles pointing to the horizontal axis in **a**. Depending on the parameter a_{12} the system can have from one to four attractors

the domains D_2: $1.55 < a_{12} \lesssim 2.1$; D_3: $a_{12} \gtrsim 2.1$; and D_4: $a_{12} < 1.55$ (Fig. 2a).

In this subsection, we assume no external input, so (8) always has a trivial solution $u^* = 0$, which corresponds to the rest state of the RDCNN. One can show that for $a_{12} \gg 1$ this solution is unique. Moreover, according to Theorem 2 it is stable since we are in D_3 and no other attractor is expected. Thus we can safely start at a big enough positive value of the collateral coupling, e.g., $a_{12} = 2.5$, and then decrease its value looking for bifurcations of steady states and limit cycles.

Figures 3a (upper panel) and 3b (phase plane 1) confirm that the rest state is the only attractor for $a_{12} = 2.5$, i.e., the RDCNN (1) is *monostable* for strong enough collateral couplings. Decreasing a_{12} we find a point where the steady state $u^* = 0$ loses stability through a Hopf bifurcation (Figs. 3a, 3b, phase plane 2). The critical coupling value is inside D_2 and depends on the delay. Using (16) and Theorem 3 we can evaluate the parameter values of the Hopf bifurcation (corresponding to τ_0^-):

$$a_{12}^* \approx 2.0356, \quad \tau^* = 1.5$$

Numerical results confirm this, also showing that the emanating limit cycle is stable in accordance with the Theorem. Thus the system stays monostable in a vicinity of $a_{12} \lesssim a_{12}^*$, but now instead of the steady state we observe stable periodic oscillations.

When decreasing further the local coupling a_{12}, the network undergoes a fold bifurcation on the frontier between the domains D_2 and D_4 ($a_{12} = 1.55$). For $\tau = 1.5$ (as in Fig. 3) the new steady states are unstable near the bifurcation point, but they become stable through Hopf bifurcations at $a_{12} \approx 1.50$. Thus for the couplings $1.16 \lesssim a_{12} \lesssim 1.50$ the RDCNN shows *tristable* behavior: depending on the initial conditions we can obtain either a periodic oscillation or one of the two nonzero steady states (Figs. 3a, 3b, phase plane 3). These nonzero steady states remain stable for any a_{12} lower than the critical value.

The three limit cycles born at corresponding three Hopf bifurcations merge together at $a \approx 1.16$ and the system undergoes a periodic orbit fold bifurcation (multiplier of the stable limit cycle crosses the unit circle at $\mu^* = 1$), such that for $-2.55 \lesssim a_{12} \lesssim 1.16$ there is a single unstable periodic orbit and two stable steady states, i.e., the network is *bistable* (Figs. 3a, 3b, phase plane 4).

At $a_{12} \approx -2.55$ the second fold bifurcation occurs leading to two new steady states. The new steady states are unstable near the bifurcation point. They undergo Hopf bifurcations at $a_{12} \approx -2.75$ with bearing unstable periodic orbits (Figs. 3a, 3b, phase plane 5). The three unstable limit cycles disappear through a double homoclinic bifurcation at $a_{12} \approx -2.78$.

Finally, at $a_{12} \approx -3.06$ two more fold bifurcations occur and we obtain nine steady states in the phase space, four of which are stable (Figs. 3a, 3b, phase plane 6). Thus for strongly negative (inhibitory) local coupling a_{12} the RDCNN is *quadristable*.

Now let us liberate the delay parameter τ and continue in 2D parameter space (a_{12}, τ) the found bifurcations. Figure 4a shows splitting of the parameter space into domains with qualitatively different behaviors of the RDCNN (1). For long enough delays ($\tau \gtrsim 0.7$) in the biophysically plausible region of collateral couplings ($0.7 \lesssim a_{12} \lesssim 2.1$) the bifurcation structure of the RDCNN is quite complex, suggesting a rich dynamics in this simple network. Besides the already discussed fold, Hopf, homoclinic, and periodic orbit fold bifurcations, for longer delays we found multiple branches of torus bifurcations (two complex multipliers cross the unit circle). The torus bifurcations enclose regions of the existence of periodic orbits born at Hopf bifurcations.

Let us for instance consider the first Hopf bifurcation (corresponding to τ_0^-). According to Theorem 3 the limit cycle emanating from the Hopf bifurcation (solid red curve marked by dots in Fig. 4a) is stable. The stability region (e.g., filled by pink in Fig. 4a) of the limit cycle from the left (smaller values of a_{12}) is bounded by the periodic orbit fold bifurcation (solid black curve marked by dots in Fig. 4a). From the right side the stability region is bounded by a torus bifurcation (solid green curve marked by dots in Fig. 4a) and the Hopf curve. The stability loss at the periodic orbit fold bifurcation has been described above and corresponds to collision and disappearance of three limit cycles (transition from inset 3 to 4 in Fig. 3b). At the torus bifurcation the limit cycle losses stability through a torus (two complex multipliers cross the unit circle).

The torus bifurcations lead to oscillatory (limit cycle) multistability in the system unobservable for shorter delay in Fig. 3. Figure 4b (left inset) shows a limit cycle and a typical trajectory approaching it, corresponding to the stable region of the limit cycle emanating from the first Hopf bifurcation (point 1 in Fig. 4a). As it follows from Theorem 4 this limit cycle corresponds to in-phase oscillation in the subnetworks A and B. Indeed, the oscillation is in-phase $y_1(t) = x_1(t)$, which we call IP_1. The subindex $m = 1$ adopted in this notation defines the sequential number of the Hopf bifurcation, which corresponds to the subindex $j = m - 1$ defining the sequence of Hopf bifurcations (see Eqs. (18)–(20) and Theorems 3, 4). Similar behavior is observed for the second Hopf bifurcation occurring at τ_1^- (solid red line marked by squares in Fig. 4a). However, in this case the bearing limit cycle corresponds to anti-phase oscillations in the subnetworks A and B (Theorem 4), denoted as AP_2. The borders of the stability region (e.g., filled by blue in Fig. 4a) of this limit cycle are given by torus bifurcations marked by squares in Fig. 4a. Figure 4b (right inset) illustrates the limit cycle for the parameter values marked by point 3 in Fig. 4a. Indeed, in the phase space this limit cycle has the relation $y_1(t) = -x_1(t)$. The latter is equivalent to $y_1(t) = x_1(t + P/2)$ given by the Theorem. Now we notice that the domains of stability of the IP_1 and AP_2 limit cycles overlap. This means that in the parameter space there exists a region (white in Fig. 4a) of coexistence of these two stable limit cycles, i.e., appearance of one or another depends on the initial conditions. Thus the RDCNN (1) is *oscillatory bistable* in this domain. Noteworthy is that in a part of this region (to the left from dashed blue curves) there are also stable steady states. Figure 4b (middle panel) shows two coexisting stable limit cycles IP_1 and AP_2 and typical trajectories approaching them.

In the parameter space there are domains with even more complex behavior. For example in the domain $\mathrm{IP}_1 + \mathrm{AP}_2 + \mathrm{IP}_3$ (filled by light green in Fig. 4a) three stable limit cycles coexist (Fig. 4c). Two of them (IP_1 and IP_3) correspond to in-phase oscillations of different shapes, while AP_2 gives anti-phase oscillations.

4.2 Switching behavior and hysteresis

Let us now illustrate some of the dynamical phenomena observable in the RDCNN that directly follow from the analysis of the bifurcation diagram shown in Fig. 4a.

First is the stability switching and alternation of in-phase and anti-phase oscillations induced by delay also discussed in Sect. 3.3 (Theorem 2). We fix the strength of the local collateral coupling $a_{12} = 2$ and change the delay τ in the interaction of the subnetworks A and B (Fig. 1b) in the range from 0.5 to 7 in seven steps each lasting 500 time units (Fig. 5, top). Other parameter values are $a_{21} = -2$ and $c = 2.05$, same as in Sect. 4.1.

Figure 5 shows the time evolution of the amplitude of oscillations in the subnetwork A, $R(t)$, and the phase difference between oscillations in the subnetworks A and B, $\Delta\varphi(t) = \varphi_A - \varphi_B$ during the whole simulation. According to the bifurcation analysis (Fig. 4a) for short delays ($\tau = 0.5$) the rest state ($u^* = 0$) is globally asymptotically stable, hence the initial perturbation of the RDCNN decays in time, $R \to 0$ (first time interval in Fig. 5). By increasing the delay to $\tau = 1.5$ we enter to the domain of the first Hopf bifurcation with in-phase oscillations IP_1 in the subnetworks A and B. This leads to an increase of the amplitude of in-phase oscillation during the second time interval. Jumping to $\tau = 2$ (interval 3 in Fig. 5) we leave the IP_1 domain (Fig. 4a) and again get monostable behavior with decaying oscillation. For $\tau = 3$ (interval 4 in Fig. 5) we enter the domain of the second Hopf bifurcation, hence observing anti-phase oscillations AP_2. Note that switching to the anti-phase oscillations is much faster than the amplitude growth. On the fifth step ($\tau = 4$) the system is again monostable and the anti-phase oscillation decays. When switching to the region IP_3

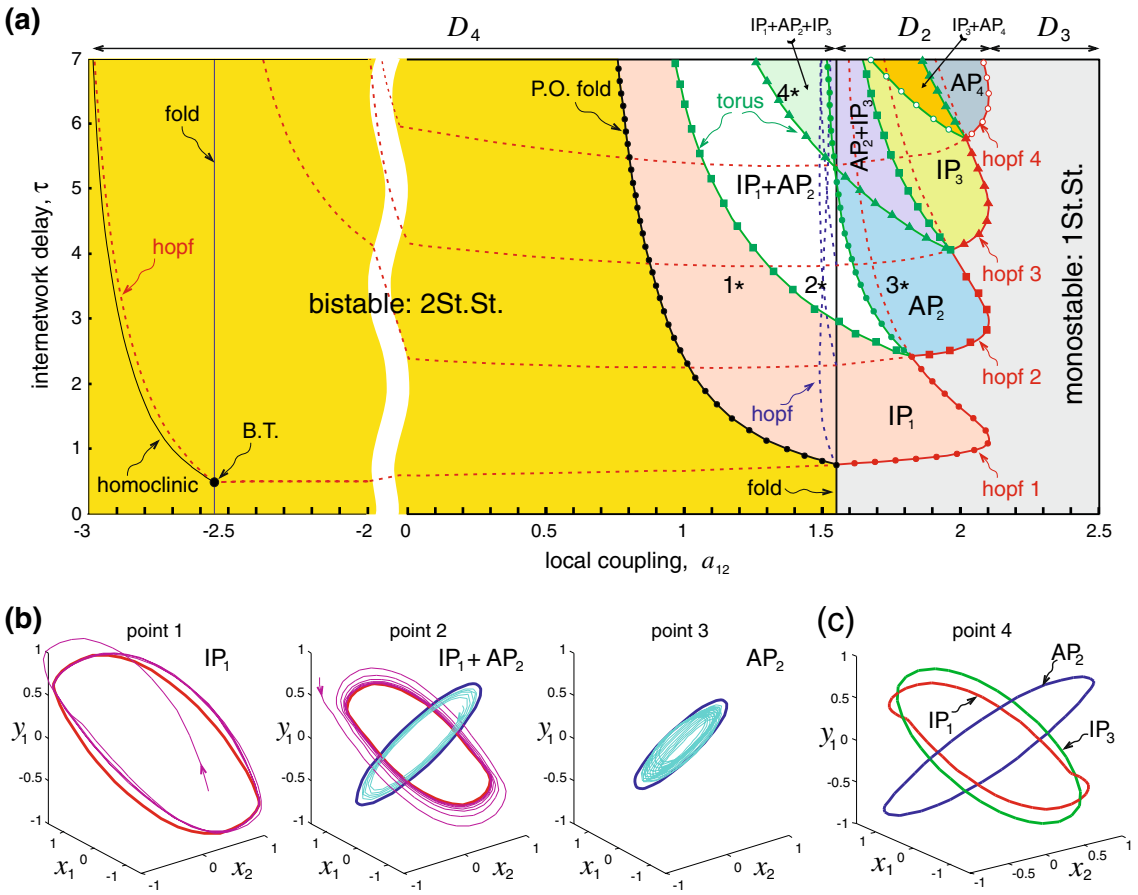

Fig. 4 **a** Complete bifurcations diagram of the RDCNN (1) (see also Fig. 3a). Branches of torus bifurcations are marked by *green lines*. *Red lines* correspond to Hopf bifurcations, *solid* and *dashed lines* are associated with stable and unstable limit cycles, respectively. *Markers* define the order of the bifurcation. *Dots* First Hopf, *squares* second Hopf, *triangles* third Hopf, and *open circles* fourth Hopf. IP and AP stand for in-phase and anti-phase oscillations in the subnetworks A and B (Fig. 1b), respectively. Subindex corresponds to the limit cycle number associated with the corresponding Hopf bifurcation. **b** Examples of projections of stable limit cycles (*thick curves*) with different spatial symmetry obtained for the parameter values marked by *stars 1, 2*, and *3* in **a** and trajectories approaching the limit cycles. *Left inset* corresponds to IP_1 (in-phase) oscillations, point 1. *Right inset* corresponds to AP_2 (anti-phase) oscillations, point 3. *Middle inset* shows two coexisting limit cycles IP_1 and AP_2, point 2. **c** Coexistence of three types of stable limit cycles (point 4 in **a**), two in-phase (IP_1 and IP_3) but of different shape and one anti-phase (AP_2)

($\tau = 5$, interval 6) the anti-phase oscillation becomes unstable and after a transient the RDCNN returns back to the in-phase regime. Finally setting $\tau = 6.5$ we again obtain an anti-phase oscillation corresponding to AP_4 in Fig. 4a. The last switching takes longer transient time. During the transients one observes phase-modulated oscillations with decreasing modulation depth.

The second phenomenon is the oscillatory hysteresis. Now we fix the delay $\tau = 4.5$ and vary quasistatically the collateral coupling a_{12} in the range [1, 2]. The RDCNN always stays oscillatory due to long enough delay (Fig. 4a), but jumps between different oscillatory patterns.

To study the hysteresis we augment the deterministic equations (1) with white Gaussian noise by adding the term $\sqrt{2D}\xi_{1,2}(t)$ to the right-hand side of equations describing the dynamics of x_1 and x_2 variables. The obtained stochastic delay differential equations were integrated by the Euler method with the time step 0.001 (lowering the step did not appreciably affect results). For $\tau = 4.5$ we can observe three different oscillation patterns IP_1, AP_2, and IP_3 (Figs. 4a, 4b). Varying a_{12} the system can enter into domains with a single stable oscillatory pattern or into domains with multiple coexisting oscillatory patterns. In the latter case the observed oscillatory pattern depends on the history, i.e., which oscillatory pattern was excited in the RDCNN before. This gives rise to the hysteresis behavior in the RDCNN (Fig. 6).

4.3 Response of the RDCNN to external stimuli

Let us now illustrate the richness and complexity of the response of the RDCNN (1) to the external input $s(t)$. Figure 7 shows four of the most prominent behaviors.

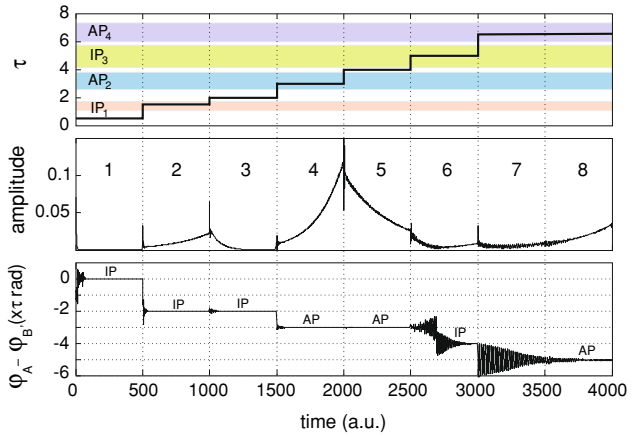

Fig. 5 Stability switches and alternation of in-phase and anti-phase oscillations induced by an increase of the delay τ. *Top* The internetwork delay as a step function changing each 500 time units. *Stripes* define different parameter domains (see also Fig. 4a). *Middle* Time evolution of the oscillation amplitude $R = \sqrt{x_1^2 + x_2^2}$. *Bottom* Phase difference between oscillations in subnetworks A and B ($\tan\varphi_A = x_2/x_1$, $\tan\varphi_B = y_2/y_1$). IP and AP stand for in-phase ($\Delta\varphi = 2\pi n$) and anti-phase ($\Delta\varphi = \pi n$, $n \neq 0$) oscillations in A and B. Parameter values: $a_{12} = 2$, $a_{21} = -2$ and $c = 2.05$

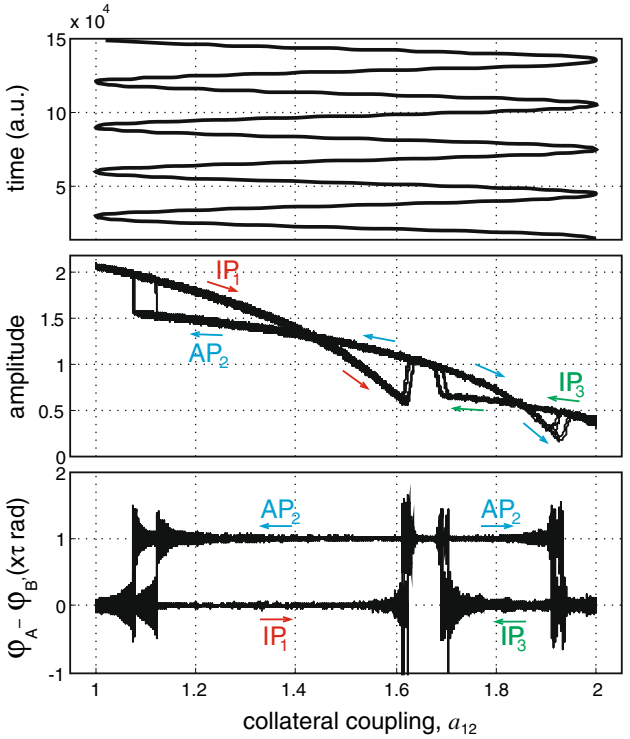

Fig. 6 Oscillatory hysteresis in the RDCNN induced by the internetwork delay $\tau = 4.5$. *Top* The collateral coupling varies quasistatically in the range $a_{12} \in [1, 2]$. *Middle* The oscillation amplitude $\|u\|$ changes slowly in the ranges of stability of in-phase ($IP_{1,3}$) and anti-phase (AP_2) limit cycles and jumps between them when the corresponding limit cycle loses stability (see also Fig 4). *Arrows* mark direction of quasistatic movements. *Bottom* Phase difference between oscillations in the subnetworks A and B. Parameter values: $a_{21} = -2$, $c = 2.05$, and $D = 2 \times 10^4$

For short enough delay values and strong collateral coupling the RDCNN is monostable (e.g., $\tau = 0.7$, $a_{12} = 1.6$ in Fig. 4a). Consequently the stimulation of the network by short lasting pulses excites decaying oscillations (Fig. 7a).

Increasing the delay we can make the RDCNN potentially oscillatory. The oscillatory behavior can be suppressed by an "hipperpolarizing" input. Then a recovering DC-input excites tonic oscillations (Fig. 7b). Depending on the delay value the emerging oscillation can be either in-phase or anti-phase in two subnetworks A and B.

The RDCNN can also detect the stimulus strength. Applying progressively increasing stimulus $s(t)$ we observed that the network oscillates in a bounded range of the stimulus strength (Fig. 7c). Moreover, in this range the oscillation amplitude depends on the stimulus strength.

Finally, appropriately selecting the network parameter values (e.g., $\tau = 3$, $a_{12} = 1.6$ in Fig. 4a, see also Fig. 6) we can have oscillatory bistability. Then applying a pulse to the RDCNN we can switch it from, e.g., anti-phase to in-phase oscillations (Fig. 7d).

5 Discussion

Communication delay between coupled units has been shown to play a significant role, generally leading to global behaviors unobservable in the absence of delay. A widely extended example is the onset of oscillations in a symmetric ring of Hopfield units when the delay (equal for all units) is above a critical (Hopf) value. Organization of sensory pathways, and particularly of the somatosensory system, suggests that interneuron delays are not symmetric and consequently their role in global dynamics may be diverse. Neurons inside spatio- and functionally-segregated regions may have negligible delays relative to the interregion delays. Besides, little is known about the influence of the delay on the SI processing by a neural network, i.e., the dynamics of the delay differential equations under an external input.

In this paper we have proposed a general system accounting for some of the major structural properties of a sensory pathway (Fig. 1). The system consists of two local subnetworks recurrently connected by feedforward and feedback couplings with delay. Neurons within each local subnetwork have no delay in their couplings. The first network also receives an external (sensory) input. Then we introduced a minimal model of the RDCNN with a pair of coupled neurons in each of the subnetworks A and B. To accommodate the known properties of the somatosensory system we assumed that the interneurons are inhibitory, while the projecting neurons are excitatory.

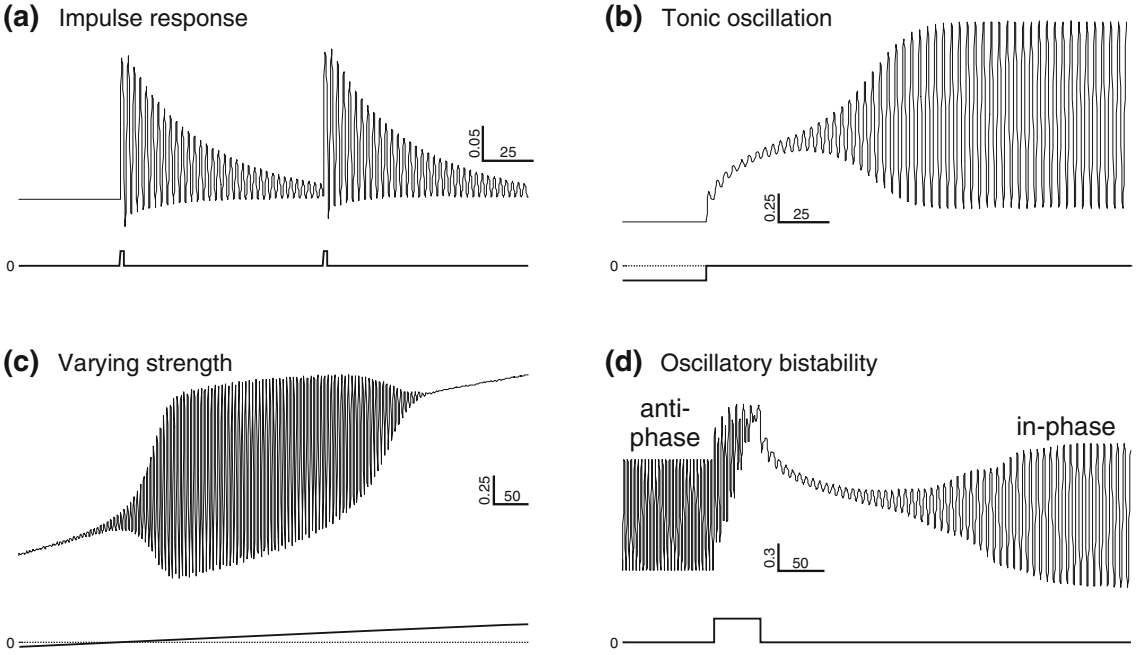

Fig. 7 Summary of the computational properties of the RDCNN. *Upper insets* show the time evolution of $x_1(t)$, while *bottom insets* show the corresponding external input $s(t)$. **a** Response to short pulses, $\tau = 0.7$. **b** Response to DC-input, $\tau = 1.6$. **c** Response to increasing strength stimulus, $\tau = 1.6$. **d** Response to a long pulse, $\tau = 3$. Other parameter values: $a_{12} = 1.6$, $a_{21} = -2$, and $c = 2.05$

We have studied the stability and bifurcations of the trivial solution $u = 0$ (or rest state of the network) and spatio-temporal patterns of bifurcating periodic oscillations in the RDCNN minimal model. By analyzing the associated characteristic equation, we found that the global dynamics of the network depends on local α and global γ (short and long term) composite gains (Theorem 2), which define the local and global synaptic properties of the network. The rest state is absolutely stable in the region D_3 of the parameter space (Fig. 2), conditionally stable in the regions D_1 and D_2, and unstable in D_4. From the SI processing viewpoint the most interesting regions (D_1, D_2, and D_3) correspond to the presence of local inhibition-excitation, i.e., in a local network one neuron should be inhibitory while the other excitatory. Such organization, i.e., excitation-inhibition local loops are widely extended in the nervous system including the somatosensory pathway (Nuñez and Malmierca 2007).

In the conditionally stable regions (D_1 and D_2) there are stability switches, i.e., the rest state is unstable in certain windows of delay values. This means that the rest state of the RDCNN can be switched from stable to unstable and back to stable and so on just by progressive increase of the delay in the feedforward and feedback couplings (Fig. 5). Such changes seem to occur in the somatosensory pathway, e.g., during development, and may be crucial for establishing the mature network structure. For instance, the response latency in the cat somatosensory cortex to forelimb stimulation over 9–29 postnatal days are about twice as long as that in adults (Bruce and Tatton 1980). The longer latency has been shown to correlate with the slower peripheral and central axonal conduction velocity, i.e., with delay, reported for young animals (see, e.g., Hildebrand and Skoglund 1971; Purpura 1973). In the motor cortex neurons show widely distributed latencies during 14–49 day period, and only small part of neurons is responsive to stimulation. Then at 50 days and older, latencies shorten markedly showing a highly modal distribution akin to the adult (Bruce and Tatton 1980). Similar results have been obtained using EEG recordings in humans. The latency of the event-related potentials of the theta rhythm decreases with increasing age in children (Yordanova and Kolev 1997). Our model results also show sensitivity of the oscillatory patterns to the delay value and to the interneuron coupling strength, and thus are inline with experimental observations showing that stimulation received in the prenatal and immediately postnatal environments may provide the input required to consolidate some of the somatosensory networks. The consolidation may consist in adjusting the delay and coupling strength (through synaptic plasticity and sensory stimulation) such that a particular neural circuit, belonging to the complete somatosensory loop, could be optimized for performing a selective information-processing task, e.g., stimulus dependent excitation of different oscillatory patterns.

Using the normal form theory and center manifold reduction, we determined the direction of the Hopf bifurcations and stability of the emanating periodic orbits (Theorem 3).

Then using the symmetric bifurcation theory of delay differential equations together with representation theory of cyclic groups we investigated the spatio-temporal patterns of these bifurcating periodic oscillations. We found different in-phase and anti-phase patterns. A remarkable finding is that spatio-temporal patterns of bifurcating periodic oscillations depend not only on the parity of critical value j, but also on the parameter region where the bifurcation occurs (Theorem 4).

In general, periodic solutions bifurcating from the Hopf bifurcation are local, i.e., they exist in a small enough neighborhood of the critical parameter value. We performed numerical studies and showed that the bifurcating periodic solutions always exist and they are orbitally asymptotically stable for $\tau \in (\tau_0^+, \tau_0^-) \cup (\tau_1^+, \tau_1^-)$. For ordinary differential equations, Mallet-Paret and Yorke (1982) have found that each source is connected to a sink by an oriented one-parameter "snake" of orbits. In our case the bifurcating periodic solutions for $\tau \in (\tau_0^+, \tau_0^-)$ or $\tau \in (\tau_1^+, \tau_1^-)$ have very similar properties.

The complete numerical bifurcation analysis of the RDCNN also has shown the presence of homoclinic, periodic orbit fold, and torus bifurcations (Fig. 4). Noteworthy is that most of the bifurcations occur in the biophysically plausible parameter region. Indeed, as a rule (e.g., for the somatosensory system Kandel et al. 2000; Nuñez and Malmierca 2007) neurons projecting to other brain areas are excitatory, which corresponds in the model (1) to positive values of the couplings a_{12}, b_{12}, c_b, and c_f, whereas interneurons that have axons inside subnetworks are usually inhibitory, i.e., $a_{21}, b_{21} < 0$ in the model. Our findings show that namely this parameter region (i.e., $a_{21} = -2$, $c = 2.05$, $a_{12} \in [1, 2.5]$, and $\tau \in [0, 6]$ in Fig. 4) contains most of the bifurcations and attractors. Thus the model inherits the adaptability and flexibility of the mimicked somatosensory system. We have shown that torus bifurcations lead to oscillatory multistability of the RDCNN, i.e., several stable limit cycles may coexist in the phase space in certain parameter regions. This explains the oscillatory hysteresis observed for quasistatic changes of the strength of the collateral coupling (Fig. 6). The oscillatory multistability may be used, e.g., as an adaptive clocking for sensory-motor commands.

The richness of the dynamical behaviors observed in the autonomous RDCNN potentially leads to a wealth of computational properties. We have shown that even the simplest RDCNN model possesses several modes of response to external stimulus (Fig. 7) from generating oscillatory pulses and tonic oscillations to changing the oscillation amplitude with stimulus strength and switching from anti-phase to in-phase oscillations. We note that nonzero delay in the internetwork communications is necessary for these regimes, similar to the well known modes of behavior of real neural assemblies.

Acknowledgments This research has been sponsored by the EU Grant SPARK II (FP7-ICT-216227), by the Spanish Ministry of Education and Science (Grants FIS2007-65173 and MEC-VEVES FIS2006-01305), by a Santander-Complutense Grant (PR41/06-15058), by the Doctoral Fund of the Ministry of Education of China (Grant 200802471024) and by NSFC (Grant 10871129).

Appendix A: Proof of Theorem 1

Let uss consider the Lyapunov functional:

$$V(u,t) = \sum_{j=1}^{4} u_j^2(t) + |c| \int_{t-\tau}^{t} \left(f^2(u_2(s)) + f^2(u_4(s)) \right) \mathrm{d}s \tag{31}$$

The time derivative of (31) using (1) in the symmetric case (7) gives

$$\begin{aligned}
\frac{\mathrm{d}V}{\mathrm{d}t} &= 2\sum_{j=1}^{4} u_j \dot{u}_j + |c| \Big\{ f^2(u_2) - f^2(u_2(t-\tau)) \\
&\qquad - f^2(u_4(t-\tau)) + f^2(u_4) \Big\} \\
&= -2\sum u_j^2 + 2c\{u_1 f(u_4(t-\tau)) + u_3 f(u_2(t-\tau))\} \\
&\quad + 2a_{12}\{u_1 f(u_2) + u_3 f(u_4)\} + 2a_{21} \\
&\quad \times \{u_2 f(u_1) + u_4 f(u_3)\} + |c| \Big\{ f^2(u_2) \\
&\quad - f^2(u_2(t-\tau)) + f^2(u_4) - f^2(u_4(t-\tau)) \Big\}
\end{aligned}$$

where to simplify notation we dropped the default argument t. Then using the inequality $2axy \le |a|(x^2 + y^2)$ one can show that

$$\begin{aligned}
\frac{\mathrm{d}V}{\mathrm{d}t} &\le -2\sum_{j=1}^{4} u_j^2 + |a_{12}| \left\{ u_1^2 + f^2(u_2) + u_3^2 + f^2(u_4) \right\} \\
&\quad + |a_{21}| \left\{ u_2^2 + f^2(u_1) + u_4^2 + f^2(u_3) \right\} \\
&\quad + |c| \left\{ u_1^2 + f^2(u_2) + u_3^2 + f^2(u_4) \right\}
\end{aligned}$$

We can rewrite

$$f(u_j(t)) = p_j(t) u_j(t)$$

where $p_j(t) = \int_0^1 f'(s u_j(t)) ds$. Due to the C^2-smoothness of f and the concavity conditions, we can find $p^* \in (0, 1]$ such that $p(t) \le p^*$ for all $t \ge 0$. Hence,

$$\begin{aligned}
\frac{\mathrm{d}V}{\mathrm{d}t} &\le -2\sum_{j=1}^{4} u_j^2 + |a_{12}|(u_1^2 + p^{*2}u_2^2 + u_3^2 + p^{*2}u_4^2) \\
&\quad + |a_{21}| \times (p^{*2}u_1^2 + u_2^2 + p^{*2}u_3^2 + u_4^2) \\
&\quad + |c|(u_1^2 + p^{*2}u_2^2 + u_3^2 + p^{*2}u_4^2)
\end{aligned}$$

$$\leq -(2-|a_{12}|-|a_{21}|-|c|)\sum_{j=1}^{4}u_j^2$$

If $|a_{12}|+|a_{21}|+|c|<2$, then we always have $dV/dt \leq 0$. Thus the Liapunov-type theorem for functional differential equations (see, e.g., Kuang 1994) ensures that the zero solution is globally asymptotically stable.

Appendix B: Main results on the roots of (13)

First let us introduce three sets of inequalities for the parameters of (13):

A1: Either $r^2 > q^2$ and $2r < p^2$, or $(2r-p^2)^2 < 4(r^2-q^2)$
A2: Either $r^2 < q^2$ or $2r > p^2$ and $(2r-p^2)^2 = 4(r^2-q^2)$
A3: $r^2 > q^2$, $2r > p^2$, and $(2r-p^2)^2 > 4(r^2-q^2)$

In addition, we denote

$$\tilde{\tau}_j^{\pm} = \begin{cases} \dfrac{1}{\omega_\pm}\left(2j\pi + \arccos\left[\dfrac{\omega_\pm^2 - r}{q}\right]\right), & pq \geq 0 \\ \dfrac{1}{\omega_\pm}\left(2(j+1)\pi - \arccos\left[\dfrac{\omega_\pm^2 - r}{q}\right]\right), & pq < 0 \end{cases} \tag{32}$$

where $j \in \{0, 1, 2, \ldots\}$ and

$$\omega_\pm = \frac{1}{\sqrt{2}}\left((2r-p^2) \pm \sqrt{(2r-p^2)^2 - 4(r^2-q^2)}\right)^{1/2} \tag{33}$$

For $\tau = 0$, (13) reduces to the second-order polynomial equation

$$\lambda^2 + p\lambda + r + q = 0 \tag{34}$$

Then the following Lemma establishes relations between the roots of Eqs. (13) and (34).

Lemma 6 (i) *If A1 holds, then the number of roots of (13) with positive real parts is the same as that of (34) for all $\tau \geq 0$.*

(ii) *If A2 holds, then the number of roots of (13) with positive real parts is the same as that of (34) for $\tau \in [0, \tilde{\tau}_0^+)$ and (13) has a pair of simple purely imaginary roots $\pm i\omega_+$ at $\tau = \tilde{\tau}_j^+$.*

(iii) *If A3 holds, then the number of roots of (13) with positive real parts is the same as that of (34) for $\tau \in [0, \min\{\tilde{\tau}_0^+, \tilde{\tau}_0^-\})$ and (13) has a pair of simple purely imaginary roots $\pm i\omega_+$ ($\pm i\omega_-$ respectively) at $\tau = \tilde{\tau}_j^+$ ($\tau = \tilde{\tau}_j^-$ respectively).*

Now substituting solution

$$\lambda(\tau) = \eta(\tau) + i\omega(\tau)$$

satisfying

$$\eta(\tilde{\tau}_j^{\pm}) = 0, \quad \omega(\tilde{\tau}_j^{\pm}) = \omega_\pm, \quad j = 0, 1, 2, \ldots$$

into (13) and taking derivatives with respect to τ, we obtain

$$\frac{d\lambda}{d\tau} = \frac{\lambda q e^{-\lambda\tau}}{2\lambda + p - \tau q e^{-\lambda\tau}} \tag{35}$$

and

$$\frac{d^2\lambda}{d\tau^2} = -\frac{2}{\lambda q e^{-\lambda\tau}}\left(\frac{d\lambda}{d\tau}\right)^3 + \frac{2}{\lambda}\left(\frac{d\lambda}{d\tau}\right)^2 - \frac{1}{\lambda}\frac{d\lambda}{d\tau}\left(\lambda + \tau\frac{d\lambda}{d\tau}\right)^2 \tag{36}$$

It follows from (35) that

$$\left.\frac{d\Re(\lambda)}{d\tau}\right|_{\tau=\tilde{\tau}_j^{\pm}} = \frac{\pm\omega_\pm^2\sqrt{(2r-p^2)^2 - 4(r^2-q^2)}}{\left(p + \tilde{\tau}_j^{\pm}(r-\omega_\pm^2)\right)^2 + (2 + p\tilde{\tau}_j^{\pm})^2\omega_\pm^2}$$

Thus, for $(2r-p^2)^2 \neq 4(r^2-q^2)$ we obtain that

$$\frac{d\Re(\lambda(\tilde{\tau}_j^+))}{d\tau} > 0, \quad \frac{d\Re(\lambda(\tilde{\tau}_j^-))}{d\tau} < 0 \tag{37}$$

and for $(2r-p^2)^2 = 4(r^2-q^2)$

$$\frac{d\Re(\lambda(\tilde{\tau}_j^+))}{d\tau} = 0 \tag{38}$$

On the other hand, from (35), we also get that for $(2r-p^2)^2 = 4(r^2-q^2)$

$$\left.\frac{d\lambda}{d\tau}\right|_{\tau=\tilde{\tau}_j^+} = iE, \quad E = -\frac{p\omega_+}{2 + p\tilde{\tau}_j^+}$$

This, together with (36), implies that if

$$(2r-p^2)^2 = 4(r^2-q^2) \quad \text{and} \quad p > 0$$

then

$$\frac{d^2\Re(\lambda(\tilde{\tau}_j^+))}{d\tau^2} = \frac{E(\omega_+ + \tilde{\tau}_j^+ E)^2}{\omega_+} + \frac{2E^3}{(\omega_+^2 - r)^2\omega_+^2 + p^2\omega_+^4} < 0 \tag{39}$$

In the case (14), the parameters $\omega_\pm$ in (33) reduce to (17). For the original characteristic equation (11) we also have

$$r^2 - q^2 = (1-\alpha)^2 - \gamma^2$$
$$2r - p^2 = -2(1+\alpha)$$
$$(2r-p^2)^2 - 4(r^2-q^2) = 4(\gamma^2 + 4\alpha)$$

Note that $p = 2 > 0$ and

$$2\pi - \arccos\left\{\frac{\omega_\pm^2 - r}{q}\right\} = \pi + \arccos\left\{\frac{\omega_\pm^2 - r}{-q}\right\}$$

Using (32), (12), (14), (16), and Lemma 6 we obtain that $\Delta_+ = 0$ is satisfied for

$$\tau = \tilde{\tau}_j^{\pm} = \tau_0^{\pm} + \begin{cases} \frac{2j\pi}{\omega_\pm}, & \text{if } \gamma > 0 \\ \frac{(2j+1)\pi}{\omega_\pm}, & \text{if } \gamma < 0 \end{cases} \tag{40}$$

and $\Delta_- = 0$ for

$$\tau = \tilde{\tau}_j^{\pm} = \tau_0^{\pm} + \begin{cases} \frac{(2j+1)\pi}{\omega_\pm}, & \text{if } \gamma > 0 \\ \frac{2j\pi}{\omega_\pm}, & \text{if } \gamma < 0 \end{cases} \tag{41}$$

where $\omega_\pm$ are given by (17). Combining (40) and (41) we arrive at (18).

Appendix C: Normal form of the system (1)

First we rescale the time $t \mapsto t/\tau$ to normalize the delay, so that the system (1) can be rewritten as a functional differential equation (FDE) in the phase space $C = C([-1, 0], \mathbb{R}^4)$. Separating the linear and nonlinear terms, (1) becomes

$$\dot{u}(t) = L_\tau(u_t) + F(u_t, \tau) \tag{42}$$

where $u_t \in C$, $u_t(\theta) = u(t + \theta)$ $(-1 \le \theta \le 0)$, and $L : C \to \mathbb{R}^4$, $F : C \to \mathbb{R}^4$ are given by

$$L_\tau(\varphi) = \tau M_1 \varphi(0) + \tau M_2 \varphi(-1) \tag{43}$$

$$F(\varphi, \tau) = \frac{\tau f'''(0)}{3!} \begin{pmatrix} a_{12}\varphi_2^3(0) + c\varphi_4^3(-1) \\ a_{21}\varphi_1^3(0) \\ a_{12}\varphi_4^3(0) + c\varphi_2^3(-1) \\ a_{21}\varphi_3^3(0) \end{pmatrix} + \mathcal{O}(|\varphi|^4) \tag{44}$$

where $\varphi = (\varphi_1, \varphi_2, \varphi_3, \varphi_4)^{\mathrm{T}} \in C$ and $M_{1,2}$ are defined by (10).

In fact, the linear map L_τ can be expressed in the integral form

$$L_\tau(\varphi) = \int_{-1}^{0} [\mathrm{d}\eta_\tau(\theta)]\varphi(\theta)$$

where $\eta_\tau : [-1, 0] \to \mathbb{R}^4 \times \mathbb{R}^4$ is a function of bounded variation defined by

$$\eta_\tau(\theta) = \tau\delta_0 M_1 - \tau\Delta_+ M_2$$

with $\delta_\nu = \delta(\theta + \nu)$ being the Dirac distribution at the point $\theta = -\nu$.

Using the bifurcation parameter μ defined in (21) (42) becomes

$$\dot{u}(t) = L_{\tau_*} u_t + \widetilde{F}(u_t, \mu) \tag{45}$$

where

$$\widetilde{F}(u_t, \mu) = L_\mu u_t + F(\varphi, \tau_* + \mu) \tag{46}$$

Let us define

$$\Omega = \omega_* \tau_* \tag{47}$$

and the associated set $\Lambda_0 = \{i\Omega, -i\Omega\}$. From Lemma 1, it follows that the characteristic equation for $\dot{u}(t) = L_{\tau_*} u_t$ has a pair of simple imaginary roots $\lambda = \pm i\Omega$ and has no other roots multiples of $\pm i\Omega$. Thus, the nonresonance conditions relative to Λ_0 are fulfilled.

Setting $C^* = C([-1, 0], \mathbb{R}^{4*})$ with $\mathbb{R}^{4*}$ being the 4D space of row vectors, we define for $\psi \in C^*$, $\phi \in C$ the adjoint bilinear form on $C^* \times C$:

$$\langle \psi(s), \phi(\theta) \rangle = \psi(0)\phi(0) - \int_{-1}^{0} \int_{0}^{\theta} \psi(\xi - \theta)\mathrm{d}\eta_{\tau_*}(\theta)\phi(\xi)\mathrm{d}\xi \tag{48}$$

Using the formal adjoint theory of FDEs (Hale et al. 1993), the phase space C can be decomposed by Λ_0 as $C = P \oplus Q$, where P is the center space for $\dot{u}(t) = L_{\tau_*} u_t$, i.e., P is the generalized eigenspace associated with Λ_0. Let Φ and Ψ be a basis for P and for the space P^* associated with the eigenvalues $\pm i\Omega$ of the formal adjoint equation, respectively, and normalized so that $\langle \Psi(s), \Phi(\theta) \rangle = I$ (I is the 4×4 identity matrix).

Using complex coordinates Φ and Ψ will be 4×4 matrices of the form:

$$\begin{aligned} &\Phi(\theta) = (\phi_1(\theta), \phi_2(\theta)) \\ &\quad \phi_1(\theta) = e^{i\Omega\theta} v, \quad \phi_2(\theta) = \overline{\phi_1(\theta)}, \quad -1 \le \theta \le 0 \\ &\Psi(s) = col(\psi_1(s), \psi_2(s)) \\ &\quad \psi_1(s) = e^{-i\Omega s} u^{\mathrm{T}}, \quad \psi_2(s) = \overline{\psi_1(s)}, \quad 0 \le s \le 1 \end{aligned} \tag{49}$$

where the over-line denotes complex conjugation, T accounts for transpose, and u, v are vectors in $\mathbb{C}^4$ such that

$$L_{\tau_*}(\phi_1) = i\Omega v, \quad u^T L(e^{i\omega_*} I) = i\Omega u^T, \quad \langle \psi_1, \phi_1 \rangle = 1 \tag{50}$$

From (40), (41), (43), (48), and (50) we can choose v and u according to the critical values, i.e., for the critical value associated with $\Delta_+ = 0$,

$$\begin{aligned} v &= \left(1, \frac{a_{21}}{i\omega_0 + 1}, -1, -\frac{a_{21}}{i\omega_0 + 1}\right)^{\mathrm{T}} \\ u &= \hat{u} \left(1, \frac{i\omega_0 + 1}{a_{21}}, -1, -\frac{i\omega_0 + 1}{a_{21}}\right)^{\mathrm{T}} \end{aligned} \tag{51}$$

and for the critical value associated with $\Delta_- = 0$,

$$\begin{aligned} v &= \left(1, \frac{a_{21}}{i\omega_0 + 1}, 1, \frac{a_{21}}{i\omega_0 + 1}\right)^{\mathrm{T}} \\ u &= \hat{u} \left(1, \frac{i\omega_0 + 1}{a_{21}}, 1, \frac{i\omega_0 + 1}{a_{21}}\right)^{\mathrm{T}} \end{aligned} \tag{52}$$

with

$$\hat{u} = \frac{1}{4 + 2\tau_* - \frac{2\tau_*\alpha}{\omega_0^2+1} + 2i\tau_*\omega_0\left(1 + \frac{\alpha}{\omega_0^2+1}\right)} \tag{53}$$

As shown in Faria and Magalhães (1995a,b), a phase space appropriate for considering normal forms of (42) is the Banach space BC of functions from $[-1, 0]$ into $\mathbb{R}^4$, which are uniformly continuous on $[-1, 0)$ and with a jump discontinuity at 0. Elements of BC have the form $\varphi + X_0 b$, where $\varphi \in C$, $b \in \mathbb{R}^4$ and $X_0(\theta)$ is defined by

$$X_0(\theta) = \begin{cases} I, & \theta = 0, \\ 0, & -r \le \theta < 0 \end{cases}$$

Let $\pi : BC \to P$ denote the projection $\pi(\varphi + X_0 b) = \Phi[\langle \Psi, \varphi\rangle + \Psi(0)b]$. Using the formal adjoint theory for FDEs, BC can be decomposed by Λ_0 as $BC = P \oplus \ker \pi$ with the property that $Q \subset \ker \pi$, where Q is an infinite dimensional complementary subspace of P in C.

Let A be the infinitesimal generator for the flow of the linear system $\dot{u}(t) = L_{\tau_*} u_t$. We decompose u_t in (42) according to the decomposition of BC, in the form $u_t = \Phi x(t) + y_t$, with $x(t) \in \mathbb{R}^2$ and $y_t \in \ker \pi \cap D(A) = Q \cap C^1 \overset{def}{=} Q^1$ where $D(A)$ is the domain of A. Let us define the 2×2 diagonal matrix

$$B = \begin{pmatrix} i\Omega & 0 \\ 0 & -i\Omega \end{pmatrix}$$

Then we can decompose (42) as

$$\begin{aligned} \dot{x} &= Bx + \Psi(0)\widetilde{F}(\Phi x + y, \mu) \\ \dot{y} &= A_{Q^1} y + (I - \pi)X_0 \widetilde{F}(\Phi x + y, \mu) \end{aligned} \tag{54}$$

where $A_{Q^1} : Q^1 \to \ker \pi$ is such that $A_{Q^1}\phi = \dot{\phi} + X_0[L_{\tau_*}(\phi) - \dot{\phi}(0)]$. Using first terms of the Taylor expansion we have

$$\begin{aligned} \Psi(0)\widetilde{F}(\Phi x + y, \mu) &\approx \frac{1}{2!} f_2^1(x, y, \mu) + \frac{1}{3!} f_3^1(x, y, \mu) \\ (I - \pi)X_0 \widetilde{F}(\Phi x + y, \mu) &\approx \frac{1}{2!} f_2^2(x, y, \mu) + \frac{1}{3!} f_3^2(x, y, \mu) \end{aligned} \tag{55}$$

where $f_j^1(x, y, \mu)$ and $f_j^2(x, y, \mu)$ are homogeneous polynomials in (x, y, μ) of degree j with coefficients in $\mathbb{C}^2$, $\ker \pi$, respectively. Therefore, (54) can be written as

$$\begin{aligned} \dot{x} &= Bx + \sum_{j \ge 2} \frac{1}{j!} f_j^1(x, y, \mu) \\ \dot{y} &= A_{Q^1} y + \sum_{j \ge 2} \frac{1}{j!} f_j^2(x, y, \mu) \end{aligned} \tag{56}$$

Since the nonresonance conditions relative to Λ_0 are satisfied, the normal form theory (Faria and Magalhães 1995a,b) implies that the center manifold locally is given by $y = 0$ and the normal form of (42) on this center manifold of the origin at $\mu = 0$ is given by

$$\dot{x} = Bx + \frac{1}{2!} g_2^1(x, 0, \mu) + \frac{1}{3!} g_3^1(x, 0, \mu) + \text{h.o.t.} \tag{57}$$

where $g_{2,3}^1(x, 0, \mu)$ are the second and third order terms in (x, μ), respectively, and h.o.t stands for higher order terms. In what follows, we explicitly derive them.

Let $V_j^3(\mathbb{C}^2)$ be the homogeneous polynomials of degree j in 3 variables, x_1, x_2, μ, with coefficients in $\mathbb{C}^2$, and let M_j^1 denote the operator from $V_j^3(\mathbb{C}^2)$ into itself defined by

$$(M_j^1 p)(x, \mu) = D_x p(x, \mu)Bx - Bp(x, \mu),$$

where $p \in V_j^3(\mathbb{C}^2)$. Then, since B is the 2×2 diagonal matrix, it follows from Faria and Magalhães (1995b) that

$$V_j^3(\mathbb{C}^2) = \text{Im}(M_j^1) \oplus \text{Ker}(M_j^1), \quad g_j^1(x, 0, \mu) \in \text{Ker}(M_j^1)$$

and

$$\begin{aligned} \text{Ker}(M_j^1) = \text{span}\Big\{ & x_1^{q_1} x_2^{q_2} \mu^l e_k : \ q_1\lambda_1 + q_2\lambda_2 = \lambda_k, \\ & k = 1, 2, \ q_1, q_2, l \in N_0, \ q_1 + q_2 + l = j \Big\} \end{aligned}$$

where $\lambda_1 = i\Omega$, $\lambda_2 = -i\Omega$ and $\{e_1, e_2\}$ is the canonical basis of $\mathbb{R}^2$. Hence,

$$\begin{aligned} \text{Ker}\,(M_2^1) &= \text{span}\left\{ \begin{pmatrix} x_1\mu \\ 0 \end{pmatrix}, \begin{pmatrix} 0 \\ x_2\mu \end{pmatrix} \right\} \\ \text{Ker}\,(M_3^1) &= \text{span}\left\{ \begin{pmatrix} x_1^2 x_2 \\ 0 \end{pmatrix}, \begin{pmatrix} x_1\mu^2 \\ 0 \end{pmatrix}, \begin{pmatrix} 0 \\ x_1 x_2^2 \end{pmatrix}, \begin{pmatrix} 0 \\ x_2\mu^2 \end{pmatrix} \right\} \end{aligned} \tag{58}$$

Since $f''(0) = 0$, by (55), we have

$$\begin{aligned} \frac{1}{2!} f_2^1(x, 0, \mu) &= \Psi(0) L_\mu(\Phi x) \\ &= \begin{pmatrix} u^{\mathrm{T}} \\ \overline{u}^{\mathrm{T}} \end{pmatrix} (L_\mu(\phi_1)x_1 + L_\mu(\phi_2)x_2) \end{aligned}$$

and the second order terms in (x, μ) of the normal form on the center manifold are given by

$$\begin{aligned} \frac{1}{2} g_2^1(x, 0, \mu) &= \frac{1}{2} \text{Proj}_{\text{Ker}(M_2^1)} f_2^1(x, 0, \mu) \\ &= \text{Proj}_{\text{Ker}(M_2^1)} \begin{pmatrix} u^{\mathrm{T}} \\ \overline{u}^{\mathrm{T}} \end{pmatrix} (L_\mu(\phi_1)x_1 + L_\mu(\phi_2)x_2) \end{aligned}$$

Note that

$$L_\mu(\phi_1) = i\mu\omega_0 v, \quad L_\mu(\phi_2) = -i\mu\omega_0 v$$

Thus

$$\frac{1}{2} g_2^1(x, 0, \mu) = \begin{pmatrix} A_1 x_1 \mu \\ \bar{A}_1 x_2 \mu \end{pmatrix} \quad \text{with} \quad A_1 = i\omega_0(u^T v).$$

From (51) and (52), we have

$$A_1 = 4i\omega_0\hat{u}. \tag{59}$$

Next we compute the cubic terms $g_3^1(x,0,\mu)$ appearing in (57). We first note that

$$\frac{1}{3!}g_3^1(x,0,\mu) = \mathrm{Proj}_{\mathrm{Ker}(M_3^1)}\frac{1}{3!}\tilde{f}_3^1(x,0,\mu) = \frac{1}{3!}\mathrm{Proj}_S\tilde{f}_3^1(x,0,0) + \mathcal{O}(|x|\mu^2)$$

for

$$S = \mathrm{span}\left\{\begin{pmatrix} x_1^2x_2 \\ 0\end{pmatrix}, \begin{pmatrix} 0 \\ x_1x_2^2\end{pmatrix}\right\}$$

where $\frac{1}{3!}\tilde{f}_3^1(x,0,\mu)$ denotes the third order terms after the computation of the normal form up to the second order terms. It is sufficient to compute only $\mathrm{Proj}_S\tilde{f}_3^1(x,0,0)$ for the purpose of determining the generic Hopf bifurcation. Since $f''(0)=0$, implying $f_2^1(x,y,0)=0$, we can deduce that, after the change of variables that transformed the quadratic terms $f_2^1(x,y,\mu)$ of the first equation in (56) into $g_2^1(x,y,\mu)$, the coefficients of third order at $y=0,\mu=0$ are still given by $\frac{1}{3!}f_3^1(x,0,0)$, i.e.,

$$\frac{1}{3!}\tilde{f}_3^1(x,0,0) = \frac{1}{3!}f_3^1(x,0,0)$$

Under the condition (4), we have $F(\varphi) = F_3(\varphi) + h.o.t.$, where F_3 is given by the first term in the r.h.s. of (44). Thus,

$$\frac{1}{3!}\tilde{f}_3^1(x,0,0) = \frac{1}{3!}f_3^1(x,0,0) = \Psi(0)F_3(\Phi x,\tau_*) = \frac{1}{3!}\tau_* f'''(0)\begin{pmatrix} u^{\mathrm{T}} \\ \overline{u}^{\mathrm{T}}\end{pmatrix} \times \begin{pmatrix} a_{12}(x_1v_2+x_2\overline{v}_2)^3 + c(x_1v_4e^{-i\Omega} \\ \quad +x_2\overline{v}_4e^{i\Omega})^3a_{21}(x_1v_1+x_2\overline{v}_1)^3 \\ a_{12}(x_1v_4+x_2\overline{v}_4)^3 + c(x_1v_2e^{-i\Omega} \\ \quad +x_2\overline{v}_2e^{i\Omega})^3a_{21}(x_1v_3+x_2\overline{v}_3)^3\end{pmatrix}$$

We have

$$\frac{1}{3!}g_3^1(x,0,0) = \frac{1}{3!}\mathrm{Proj}_S\tilde{f}_3^1(x,0,0) = \begin{pmatrix} A_2x_1^2x_2 \\ \bar{A}_2x_1x_2^2\end{pmatrix}$$

where

$$A_2 = \frac{1}{2}\tau_* f'''(0)\left(a_{12}u_1v_2|v_2|^2 + a_{21}u_2v_1|v_1|^2 + a_{12}u_3v_4|v_4|^2 + a_{21}u_4v_3|v_3|^2 + c(u_1v_4|v_4|^2 + u_3v_2|v_2|^2)e^{-i\omega_*}\right)$$

This together with (51) and (52) yield

$$A_2 = \frac{1}{2}f'''(0)\tau_*\|v\|^2(1+i\omega_0)u_1. \tag{60}$$

Thus, the normal form (57) becomes

$$\dot{x} = Bx + \begin{pmatrix} A_1x_1\mu \\ \bar{A}_1x_2\mu\end{pmatrix} + \begin{pmatrix} A_2x_1^2x_2 \\ \bar{A}_2x_1x_2^2\end{pmatrix} + \mathcal{O}\left(|x|\mu^2 + |x^4|\right), \tag{61}$$

where A_1 and A_2 are defined by (59) and (60), respectively. Introducing polar coordinates (ϱ,ξ): $(x_2+x_1)/2 = \varrho\cos\xi$, $(x_2-x_1)/2 = \varrho\sin\xi$, we obtain the normal form (22).

Appendix D: Proof of Lemma 4

From (51), (52) and (27), we have

$$\rho(\Re(v)) = \begin{cases} -\Re(v) & \text{for } \Delta_+ = 0 \\ \Re(v) & \text{for } \Delta_- = 0\end{cases}$$

$$\rho(\Im(v)) = \begin{cases} -\Im(v) & \text{for } \Delta_+ = 0 \\ \Im(v) & \text{for } \Delta_- = 0\end{cases}$$

Consequently,

$$\begin{aligned}&\rho(x_1\varepsilon_1(t)+x_2\varepsilon_2(t)) = \\ &\quad x_1\left[\cos\left(\frac{2\pi}{\omega}t\right)\rho(\Re(v)) - \sin\left(\frac{2\pi}{\omega}t\right)\rho(\Im(v))\right] \\ &\quad +x_2\left[\sin\left(\frac{2\pi}{\omega}t\right)\rho(\Re(v)) + \cos\left(\frac{2\pi}{\omega}t\right)\rho(\Im(v))\right] \\ &= \begin{cases} -(x_1\varepsilon_1(t)+x_2\varepsilon_2(t)) & \text{for } \Delta_+ = 0 \\ x_1\varepsilon_1(t)+x_2\varepsilon_2(t) & \text{for } \Delta_- = 0\end{cases}\end{aligned}$$

and

$$\begin{aligned}&x_1\varepsilon_1(t+\theta)+x_2\varepsilon_2(t+\theta) \\ &= x_1\left[\cos\left(\frac{2\pi}{\omega}t\right)\cos\left(\frac{2\pi}{\omega}\theta\right) - \sin\left(\frac{2\pi}{\omega}t\right)\sin\left(\frac{2\pi}{\omega}\theta\right)\right]\Re(v) \\ &\quad -x_1\left[\sin\left(\frac{2\pi}{\omega}t\right)\cos\left(\frac{2\pi}{\omega}\theta\right) + \cos\left(\frac{2\pi}{\omega}t\right)\sin\left(\frac{2\pi}{\omega}\theta\right)\right]\Im(v) \\ &\quad +x_2\left[\sin\left(\frac{2\pi}{\omega}t\right)\cos\left(\frac{2\pi}{\omega}\theta\right) + \cos\left(\frac{2\pi}{\omega}t\right)\sin\left(\frac{2\pi}{\omega}\theta\right)\right]\Re(v) \\ &\quad +x_2\left[\cos\left(\frac{2\pi}{\omega}t\right)\cos\left(\frac{2\pi}{\omega}\theta\right) - \sin\left(\frac{2\pi}{\omega}t\right)\sin\left(\frac{2\pi}{\omega}\theta\right)\right]\Im(v) \\ &= \left(x_1\cos\left(\frac{2\pi}{\omega}\theta\right) + x_2\sin\left(\frac{2\pi}{\omega}\theta\right)\right)\varepsilon_1(t) \\ &\quad + \left(-x_1\sin\left(\frac{2\pi}{\omega}\theta\right) + x_2\cos\left(\frac{2\pi}{\omega}\theta\right)\right)\varepsilon_2(t)\end{aligned}$$

Thus in order for the following equality

$$\rho(x_1\varepsilon_1(t)+x_2\varepsilon_2(t))=x_1\varepsilon_1(t+\theta)+x_2\varepsilon_2(t+\theta) \qquad (62)$$

to hold, we must have, for $\Delta_+=0$,

$$x_1\cos\left(\frac{2\pi}{\omega}\theta\right)+x_2\sin\left(\frac{2\pi}{\omega}\theta\right)=-x_1$$
$$-x_1\sin\left(\frac{2\pi}{\omega}\theta\right)+x_2\cos\left(\frac{2\pi}{\omega}\theta\right)=-x_2$$

and, for $\Delta_-=0$,

$$x_1\cos\left(\frac{2\pi}{\omega}\theta\right)+x_2\sin\left(\frac{2\pi}{\omega}\theta\right)=x_1$$
$$-x_1\sin\left(\frac{2\pi}{\omega}\theta\right)+x_2\cos\left(\frac{2\pi}{\omega}\theta\right)=x_2$$

Thus (62) holds if and only if

$$\theta=\left(k+\frac{1}{2}\right)\omega, \quad \text{for } \Delta_+=0, \text{ or}$$
$$\theta=k\omega, \quad \text{for } \Delta_-=0, \text{ or}$$
$$x_1=x_2=0, \quad \text{otherwise}$$

where $k\in\mathbb{Z}$. This completes the proof.

Appendix E: Proof of Lemma 5

According to Golubitsky et al. (2003), $\mathbb{R}$ is an absolutely irreducible representation of Γ. It follows from (50) that

$$\mathrm{Ker}\Delta(\tau_*,i\omega_0)=\{(y_1+iy_2)v;\quad y_1,y_2\in\mathbb{R}\}$$

Define

$$J((y_1+iy_2)v)=(y_1,y_2)^{\mathrm{T}}$$

Clearly, $J:\mathrm{Ker}\Delta(\tau_*,i\omega_0)\cong\mathbb{R}^2$ is a linear isomorphism. Note that

$$\rho((y_1+iy_2)v)=(y_1+iy_2)\rho(v)$$
$$=\begin{cases}-(y_1+iy_2)v & \text{for } \Delta_+=0\\ (y_1+iy_2)v & \text{for } \Delta_-=0\end{cases}$$

Consequently,

$$J[\rho((y_1+iy_2)v)]=\rho[J((y_1+iy_2)v)]$$

which completes the proof.

References

Braitenberg V, Schuz A (1998) Cortex: statistics and geometry of neuronal connectivity. Springer, Berlin

Bruce IC, Tatton WG (1980) Sequential output-input maturation of kitten motor cortex. Exp Brain Res 39:411–419

Bungay S, Campbell SA (2007) Patterns of oscillation in a ring of identical cells with delayed coupling. Int J Bifurcat Chaos 17: 3109–3125

Campbell SA, Edwards R, Van den Driessche P (2004) Delayed coupling between two neural network loops. SIAM J Appl Math 65:316–335

Campbell SA, Yuan Y, Bungay SD (2005) Equivariant Hopf bifurcation in a ring of identical cells with delayed coupling. Nonlinearity 18:2827–2846

Castellanos NP, Malmierca E, Nuñez A, Makarov VA (2007) Corticofugal modulation of the tactile response coherence of projecting neurons in the gracilis nucleus. J Neurophysiol 98:2537–2549

Chow S-N, Hale JK (1982) Methods of bifurcation theory. Springer, New York

Engelborghs K, Luzyanina T, Samaey G (2001) DDE-BIFTOOL v. 2.00: a Matlab package for bifurcation analysis of delay differential equations. Technical Report TW-330, Department of Computer Science, K.U. Leuven, Leuven, Belgium

Ernst U, Pawelzik K, Geisel T (1995) Synchronization induced by temporal delays in pulse-coupled oscillators. Phys Rev Lett 74: 1570–1573

Faria T, Magalhães LT (1995a) Normal form for retarded functional differential equations with parameters and applications to Hopf bifurcation. J Differ Equ 122:181–200

Faria T, Magalhães LT (1995b) Normal form for retarded functional differential equations and applications to Bogdanov–Takens singularity. J Differ Equ 122:201–224

Fuchs A, Haken H (1988) Pattern recognition and associative memory as dynamical processes in nonlinear systems. Neural Netw 1: 217–224

Gerstner W (1996) Rapid phase locking in systems of pulse-coupled oscillators with delay. Phys Rev Lett 76:1755–1758

Golubitsky M, Stewart I, Schaeffer D (2003) Singularities and groups in bifurcation theory, vol II. Springer, New York

Guo S (2005) Spatio-temporal patterns of nonlinear oscillations in an excitatory ring network with delay. Nonlinearity 18:2391–2407

Guo S (2007) Stability of nonlinear waves in a ring of neurons with delays. J Differ Equ 236:343–374

Guo S, Huang L (2003) Hopf bifurcating periodic orbits in a ring of neurons with delays. Physica D 183:19–44

Hale JK, Verduyn Lunel SM (1993) Introduction to functional differential equations. Springer, New York

Hildebrand C, Skoglund S (1971) Calibre spectra of some fibre tract in the feline central nervous system during postnatal development. Acta Physiol Scand (Suppl) 364:5–41

Huang L, Wu J (2003) Nonlinear waves in networks of neurons with delayed feedback: pattern formation and continuation. SIAM J Math Anal 34:836–860

Ikeda K, Matsumoto K (1987) High-dimensional chaotic behavior in systems with time-delayed feedback. Physica D 29:223–235

Jabbur SJ, Towe AL (1961) Analysis of the antidromic cortical response following stimulation at the medullary pyramids. J Physiol 155: 148–160

Kandel ER, Schwartz JH, Jessell TM (2000) Principles of neural science, 4th edn. McGraw-Hill, New York

Kuang Y (1994) Delay differential equations with applications in population dynamics. Academic Press, Boston

Makarov VA, Makarova J, Herreras O (2009) Deconvolution of local field potential sources by independent component analysis. J Comput Neurosci (submitted)

Mallet-Paret J, Yorke JA (1982) Oriented families of periodic orbits, their sources, sinks and continuation. J Differ Equ 43: 419–450

Malmierca E, Castellanos NP, Nunez A, Makarov VA, Nuñez A (2009) Neuron synchronization in the rat gracilis nucleus facilitates sensory transmission in the somatosensory pathway. Eur J Neurosci (accepted)

Marcus CM, Westervelt RM (1989) Stability of analog neural networks with delay. Phys Rev A 39:347–359

Niebur E, Schuster HG, Kammen D (1991) Collective frequencies and metastability in networks of limit-cycle oscillators with time delay. Phys Rev Lett 67:2753–2756

Nuñez A, Malmierca E (2007) Corticofugal modulation of sensory information. Advances in anatomy embryology and cell biology, vol 187. Springer, Berlin

Purpura DP (1973) Analysis of morphophysiological developmental processes in mammalian brain. Res Publ Assoc Nerv Ment Dis 51:79–110

Ramana Reddy DV, Sen A, Johnston GL (1998) Time delay induced death in coupled limit cycle oscillators. Phys Rev Lett 80: 5109–5112

Ramana Reddy DV, Sen A, Johnston GL (1999) Time delay effects on coupled limit cycle oscillators at Hopf bifurcation. Physica D 129:15–34

Ruan S (2001) Absolute stability, conditional stability and bifurcation in Kolmogorov-type predator-prey systems with discrete delays. Q Appl Math 59:159–173

Schuster HG, Wagner P (1989) Mutual entrainment of two limit cycle oscillators with time delayed coupling. Prog Theor Phys 81: 939–945

Seunghwan K, Seon H, Ryu CS (1997) Multistability in coupled oscillator systems with time delay. Phys Rev Lett 79:2911–2914

Song Y, Han M, Peng Y (2004) Stability and Hopf bifurcations in a competitive Lotka-Volterra system with two delays. Chaos Solitons Fractals 22:1139–1148

Song Y, Han M, Wei J (2005) Stability and Hopf bifurcation analysis on a simplified BAM neural network with delays. Physica D 200:185–204

Song Y, Wei J, Yuan Y (2007) Stability switches and Hopf bifurcations in a pair of delay-coupled oscillators. J Nonlinear Sci 17:145–166

Timme M, Wolf F, Geisel T (2002a) Prevalence of unstable attractors in networks of pulse-coupled oscillators. Phys Rev Lett 89: 154105-1-4

Timme M, Wolf F, Geisel T (2002b) Coexistence of regular and irregular dynamics in complex networks of pulse-coupled oscillators. Phys Rev Lett 89:258701-1-4

Valverde F (1966) The pyramidal tract in rodents. A study of its relations with the posterior column nuclei, dorsolateral reticular formation of the medulla, and cervical spinal cord (Golgi and E.M. observations). Zeit f Zellforsch 71:297–363

Wei J, Velarde MG (2004) Bifurcation analysis and existence of periodic solutions in a simple neural network with delays. Chaos 14:940–953

Wei J, Velarde MG, Makarov VA (2002) Oscillatory phenomena and stability of periodic solutions in a simple neural network with delay. Nonlinear Phenom Complex Syst 5:407–417

Wen Q, Chklovskii DB (2005) Segregation of the brain into gray and white matter: A design minimizing conduction delays. PLoS Comput Biol 1:617–630

Wu J (1998) Symmetric functional-differential equations and neural networks with memory. Trans Am Math Soc 350:4799–4838

Wu J, Faria T, Huang YS (1999) Synchronization and stable phase-locking in a network of neurons with memory. Math Comput Model 30:117–138

Yordanova J, Kolev V (1997) Developmental changes in the event-related EEG theta response and P300. Electroencephalogr Clin Neurophysiol 104:418–430

Yuan Y (2007) Dynamics in a delayed-neural network. Chaos Solitons Fractals 33:443–454

Yuan Y, Campbell SA (2004) Stability and synchronization of a ring of identical cells with delayed coupling. J Dyn Differ Equ 16: 709–744